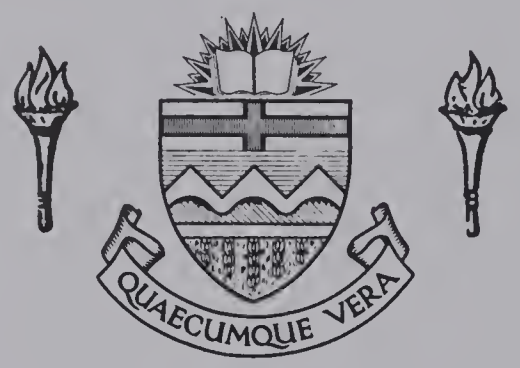

THE UNIVERSITY OF ALBERTA

DOPPLER SHIFT LIFETIME MEASUREMENTS

BY

© PAUL RAMSDEN HENRYK GUTOWSKI

A THESIS

SUBMITTED TO THE FACULTY OF GRADUATE STUDIES

IN PARTIAL FULFILMENT OF THE REQUIREMENTS FOR THE DEGREE

OF MASTER OF SCIENCE

DEPARTMENT OF PHYSICS

EDMONTON, ALBERTA

FALL, 1970

UNIVERSITY OF ALBERTA

FACULTY OF GRADUATE STUDIES

The undersigned certify that they have read, and recommend to the Faculty of Graduate Studies for acceptance, a thesis entitled DOPPLER SHIFT LIFETIME MEASUREMENTS submitted by Paul Ramsden Henryk Gutowski in partial fulfilment of the requirements for the degree of Master of Science.

ABSTRACT

Lifetimes for the 1288 KeV and the 1440 KeV levels of ^{53}Mn were measured using the Doppler shift attenuation method through the ^{53}Cr (p, nγ) ^{53}Mn reaction with a proton energy of 5.20 MeV. The lifetime of the 1288 KeV level was determined to be $1.5\ ^{+\infty}_{-1.3}$ p.s. and that of the 1440 KeV level was found to be $8.0\ ^{+\infty}_{-7.7}$ p.s. .

The Doppler shift attenuation method is discussed in Chapter 1 with the evaluation of the F(τ) function. The mechanism of pulse shape variation with incident radiation in liquid organic scintillators and pulse shape distributions in Ge (Li) detectors with their timing effects are discussed in Chapter 2. In Chapter 3 the electronics system and experimental arrangement are explained. Chapter 4 examines the method of data analysis and the results of the ^{53}Mn lifetime experiment are presented and discussed in Chapter 5.

ACKNOWLEDGEMENTS

I would like to take this opportunity of expressing my thanks and appreciation to the following persons who were instrumental in the completion of this work:

To my supervisor, Dr. W.C. Olsen, for his encouragement and help during the last two years of my undergraduate program and the first year of my graduate career, and for introducing me to lifetime work.

To my acting supervisor, Dr. G.C. Neilson, for suffering my bad writing throughout a rather voluminous text and for his help and guidance during the terminal stages of this work.

To Dr. W.J. McDonald who kept me from stubbing my toe.

To Dr. B.C. Robertson, special thanks for his constant, never-failing encouragement, advice, and assistance in virtually every phase of this work from the actual running of the experiment to the final discussions of the results. Merci, Barry.

To Georges for involving me in gamma ray work.

To Ed Wong for his help in running the experiment and for the discussions involving data analysis.

To my other colleagues in the gamma ray group - Peter Green (Polarimeter Peter), Jim Pasos (Midnight Jim), and Woon Chung (who has to carry on with ^{53}Mn) - many thanks.

To Uncle Jock and the staff of the NRC who kept the machine "alive" if not "well".

To Mrs. Mary Yiu who did such a beautiful job in the typing of the manuscript despite my bad writing and my multitude of equations.

TABLE OF CONTENTS

LIST OF TABLES

LIST OF FIGURES

CHAPTER 1

THE DOPPLER SHIFT ATTENUATION MEASUREMENT METHOD (DSAM)

1.1 The principle behind the determination of nuclear lifetimes by studying the Doppler shift or broadening of gamma rays from the de-excitation of nuclear levels is based on the rapid slowing down of moving atoms in a solid. These swiftly moving atoms have a characteristic slowing down time of the order of 10^{-13} sec. in most solids (that is, the time required for the velocity of the moving atom to decrease to one-half its initial value). The nature of the function of velocity with respect to time is a decreasing exponential, but the explicit function can only be determined through a detailed examination of the processes involved in the stopping of atoms or ions in solid materials. Having done this, however, one has a clock by which one can compare the lifetimes of nuclear levels. At present the method can be used to determine lifetimes of the order 10^{-11} sec. to 10^{-14} sec. and is limited by the ability of the detection system to resolve small Doppler shifts.

The energy of a gamma ray from the de-excitation of a nucleus moving at a velocity $\vec{v}$ with respect to an observer is given by

$$E_\gamma = E_{\gamma o} \left(1 + \frac{v}{c} \cos \theta\right) \qquad (1)$$

or $$\Delta E_\gamma = E_{\gamma o} \frac{v}{c} \cos \theta \qquad (2)$$

which is accurate to first order in $\frac{v}{c}$ since the velocities here are less than 1% of c, the velocity of light. $E_{\gamma o}$ is the energy of the unshifted gamma ray and θ is the instantaneous direction of travel at de-excitation and is measured from the initial beam direction.

Suppose, now, the situation is as depicted in figure 1 where a proton in the beam collides with a target nucleus which ejects a neutron and forms a recoil nucleus in an excited state. If the recoil nucleus decays by emitting a gamma ray after a time τ (lifetime) then it will have slowed down from some initial recoil velocity $\vec{v}_o$ to some velocity $\vec{v}_d$ by encounters with atoms in the target or backing material. Clearly $\vec{v}_d = \vec{v}_d(\tau)$.

Therefore, $$\Delta E_\gamma = E_{\gamma o} \frac{v_d}{c} \cos \theta \qquad (3)$$

or $$\Delta E_\gamma = E_{\gamma o} \frac{v_d}{v_o} \frac{v_o}{c} \cos \theta \qquad (4)$$

$$= E_{\gamma o} \frac{v_o}{c} \frac{v_d}{v_o} \cos(\overset{0}{0}) \qquad (5)$$

for the simple case of a straight-on recoil. $E_{\gamma o} \frac{v_o}{c}$ is the maximum possible Doppler shift for an infinitely

Figure 1. A proton (p) enters the target material (in this case also the stopping material) and strikes a ^{53}Cr nucleus forming a compound nucleus which decays into a neutron (n) and a ^{53}Mn recoil nucleus (A) in an excited state. The recoil nucleus then slows down in the stopping material.

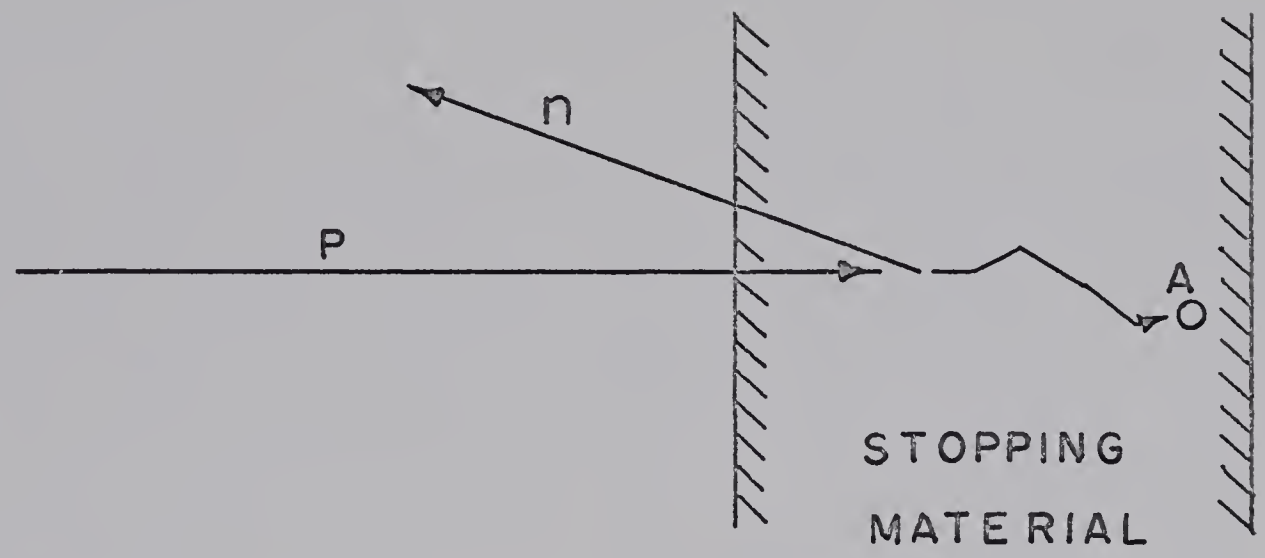

FIGURE 1

Figure 2. $\vec{v}(t)$ is the velocity of the recoil nucleus (located at the origin). $\vec{d}$ is the vector pointing in the direction of the gamma ray detector. The polar angles for $\vec{v}(t)$ and $\vec{d}$ respectively are θ_2 and θ_1, the azimuthal angles being ϕ_2 and ϕ_1. $\vec{v}_o$ is the initial velocity of the recoil nucleus.

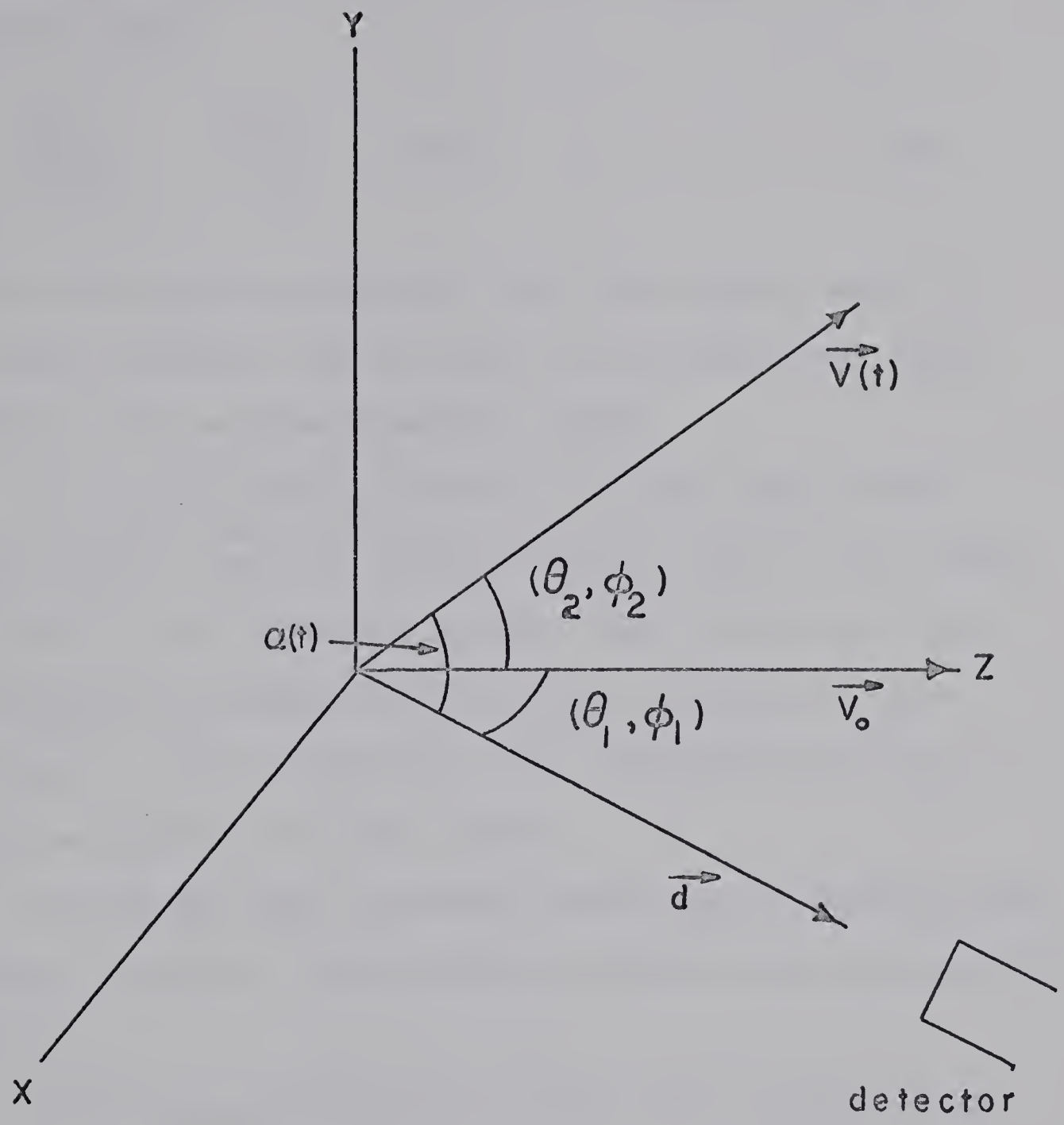

FIGURE 2

short nuclear lifetime and one defines $\Delta E_{\gamma o} \equiv E_{\gamma o} \frac{v_o}{c}$. The ratio, then,

$$\frac{\Delta E_\gamma}{\Delta E_{\gamma o}} = \frac{v_d(\tau)}{v_o} \equiv F(\tau) \qquad (6)$$

is the attenuation resulting from the slowing down of the recoil nucleus, and is equal to the observed shift divided by the maximum possible shift.

In general, the situation is more complicated and the actual shift is determined not only by the speed $v_d(\tau)$ but by the angle of recoil. The scattered nuclei are distributed symmetrically about the initial beam direction (z axis) and,hence, the averaged direction of recoil is parallel to the z axis.

One knows that a nucleus recoiling in some excited state of lifetime τ decays with a probability proportional to $e^{-t/\tau}$.

It is assumed that the recoil ion travels in an initial direction denoted by the z axis and that at the time of emission of a gamma ray in a direction $\vec{d}$ the recoil ion is travelling with a velocity $\vec{v}(t)$ making an angle α with $\vec{d}$. $\vec{d}$ is described by the polar angle θ_1 and the azimuthal angle ϕ_1 (which is zero here because of the choice of the coordinate system). The direction of $\vec{v}$ is specified by θ_2 and ϕ_2 (figure 2).

The projection of $\vec{v}(t)$ on the line of observation is $\vec{v}(t) \cdot \vec{d}$ or $v(t) \cos \alpha(t)$. Therefore, the Doppler shift is given by the integral of this product weighted by the probability for decay of the nucleus over all time (Ro 69):

$$\Delta E_\gamma = \frac{E_{\gamma o}}{c} \int_0^\infty v(t) \cos \alpha(t) \exp(-t/\tau)\, dt \ . \quad (7)$$

For a number of such events, j, all of liftime τ and speed $v(t)$, and each with angle $\alpha_j(t)$, the average Doppler shift (over N such events) becomes

$$\overline{\Delta E_\gamma} = \frac{1}{N} \frac{E_{\gamma o}}{c} \sum_{j=1}^{N} \int_0^\infty v(t) \cos \alpha_j \exp(-t/\tau) dt \ . \quad (8)$$

Using the fact that $P_1(\cos \alpha) = \cos \alpha$ and the addition theorem of spherical harmonics;

$$P_\ell(\cos \alpha) = \frac{4\pi}{2\ell+1} \sum_{M=-\ell}^{\ell} Y_\ell^{M*}(\theta_1, \phi_1)\, Y_\ell^{M}(\theta_2, \phi_2) \ ,$$

one has for the average Doppler shift

$$\overline{\Delta E_\gamma} = \frac{E_{\alpha o}}{Nc} \sum_{j=1}^{N} \int_0^\infty v(t) \left(\frac{4\pi}{2\ell+1}\right) \sum_{M=-\ell}^{\ell} Y_1^{M*}(\theta_1, 0)\, Y_1^{M}(\theta_2, \phi) \times \exp(-t/\tau)\, dt \quad (9)$$

where the values $\phi_1 = 0$ and $\phi_2 = \phi$ have been used (ϕ is randomly distributed by reason of axial symmetry).

The probability, P, of an event occurring in the interval between ϕ_j and $\phi_j + d\phi$ is proportional to $d\phi$, or, if P is normalized to unity over the full range of ϕ $(=2\pi)$,

$$P = d\phi/(\int_0^{2\pi} d\phi) = d\phi/2\pi \quad . \tag{10}$$

Therefore, for very large N, corresponding to a large number of nuclei decaying at the same time giving off gamma rays of energy $E_{\gamma o}$ in their rest frames, one has:

$$\frac{1}{N} = d\phi/2\pi \tag{11}$$

and, hence, the summation $\frac{1}{N} \sum_{j=1}^{N}$ may be replaced by the integral $\frac{1}{2\pi} \int_0^{2\pi} d\phi$.

Expression (9), therefore becomes

$$\overline{\Delta E_\gamma} = \frac{E_{\gamma o}}{c} \int_0^\infty v(t) \left(\frac{2}{2\ell+1}\right) \int_0^{2\pi} \sum_M Y_1^M(\theta_2(t),\phi)\ Y_1^{M*}(\theta_1,0)\ d\phi$$

$$\times \exp(-t/\tau)\ dt \quad . \tag{12}$$

Using the well-known formulae,

$$Y_\ell^M(\theta,\phi) = (-1)^M \left[\frac{2\ell+1}{4\pi} \frac{(\ell-M)!}{(\ell+M)!}\right]^{\frac{1}{2}} P_\ell^M(\cos\theta) \exp(iM\phi)$$

and, $Y_{\ell}^{M*}(\theta,\phi) = (-1)^{M} Y_{\ell}^{-M}(\theta,\phi)$

one has for (12)

$$\overline{\Delta E_{\gamma}} = \frac{E_{\gamma o}}{c} \int_0^{\infty} v(t) \left(\frac{2}{2\ell+1}\right) \int_0^{2\pi} \sum_{M=-\ell}^{\ell} \frac{2\ell+1}{4\pi} P_1^{-M}(\cos\theta_1) P_1^{M}(\cos\theta_2(t))$$

$$\times \exp(iM\phi)\, d\phi \exp(-t/\tau)\, dt \,. \qquad (13)$$

Clearly, if $\overline{\Delta E_{\gamma o}}$ is to be non-zero then M = 0 and one has

$$\overline{\Delta E_{\gamma}} = \frac{E_{\gamma o}}{c} P_1(\cos\theta_1) \int_0^{\infty} v(t)\, P_1(\cos\theta_2(t)) \exp(-t/\tau)\, dt$$

$$= \frac{E_{\gamma o}}{c} \cos\theta_1 \int_0^{\infty} v(t) \cos\theta_2(t) \exp(-t/\tau)\, dt \,. \qquad (14)$$

Of course, initially the recoil ions are moving with velocity $\vec{v}_o$ (along the z axis) and so the maximum Doppler shift for these ions are given by

$$\Delta E_{\gamma o} = \frac{E_{\gamma o}}{c} \int_0^{\infty} \vec{v}_o . \vec{d} \exp(-t/\tau)\, dt \qquad (15)$$

using (7) with $\vec{v}(t) = \vec{v}_o$, a constant. Or

$$\Delta E_{\gamma o} = \frac{E_{\gamma o}}{c} \int_0^{\infty} v_o \cos\theta_1 \exp(-t/\tau)\, dt \qquad (16)$$

where the expression $\vec{v}_o . \vec{d} = v_o \cos\theta_1$ has been used. From the previous definition of $F(\tau)$ one has:

$$F(\tau) = \frac{\overline{\Delta E_\gamma}}{\Delta E_{\gamma o}} = \frac{\int_0^\infty v(t) \cos \overline{\phi(t)} \exp(-t/\tau)\, dt}{\int_0^\infty v_o \exp(-t/\tau)\, dt} \qquad (17)$$

where $\theta_2(t) \equiv \overline{\phi(t)}$. According to convention one defines $\cos \overline{\phi(t)}$ to be $\overline{\cos \phi(t)}$ which projects the average velocity $\overline{\vec{v}(t)}$ onto the z axis which is the initial direction of travel.

1.2 In order to determine the velocity function, v(t), it is necessary to know the stopping power $\frac{dE}{dx}$ of the slowing-down material. E, of course, is the energy of the recoiling ion and x is its distance traversed.

From simple mechanics one has

$$E = P^2/2M \qquad (18)$$

where P is the momentum of the ion and M its mass. Therefore,

$$\frac{dE(v)}{dx} = \frac{1}{M} \frac{dP}{dx} \quad P = M \frac{dv}{dx} v$$

$$= M \frac{dv}{dx} \cdot \frac{dx}{dt}$$

$$= M \frac{dv(t)}{dt} \quad . \qquad (19)$$

Hence,

$$dt = \frac{M\, dv}{\frac{dE(v)}{dx}} \qquad (20)$$

can be used to derive v(t). $\frac{dE(v)}{dx}$ is usually given in units of $KeV.cm^2/mg$ and since, dimensionally,

$$MeV.cm^{-1} = (KeV.cm^2.mg^{-1}) \times (g.cm^{-3})$$

(the last factor on the right is clearly the density of the material, ρ)

$$\frac{dE}{dx'} (MeV.cm^{-1}) = \frac{dE}{dx} (KeV.cm^2.mg^{-1}) \qquad (21)$$

and $$x = x'\rho \qquad (22)$$

in transferring from one system of units to another. $\frac{dE}{dx}$ can be broken down into the sum of two distinct processes: electronic and nuclear stopping. That is,

$$\frac{dE}{dx} = (\frac{dE}{dx})_e + (\frac{dE}{dx})_n \qquad (23)$$

where the subscripts e and n refer to the electronic and nuclear processes respectively.

Electronic stopping , the mechanism of which is essentially the collision between electrons from the surrounding medium and the recoiling ion, is a continuous process since each individual encounter with the electron cloud involves an energy loss of the order 10 z_2 electron volts (No 63), where z_2 is the atomic number of the stopping atom, which is much smaller than the recoil

energy of the nucleus which is of the order of 0.1 MeV. Hence, this process does not involve changes in the recoil direction. Nuclear encounters, which take place at much lower energies than the initial recoil energy ($137 \frac{v_c}{c} << 1$, where v_c is the velocity of the ion when nuclear stopping becomes larger than electronic stopping) (No 63), involve large direction changes which are manifested by the $\overline{\cos \phi(t)}$ term in the expression (17) for $\overline{\Delta E_\gamma}$.

1.3 Electronic Stopping

One can gain insight into the behavior of the electronic stopping process involving the encounter between a moving ion and the electron cloud surrounding the atoms of the stopping material by considering this cloud to be a degenerate electron gas. That is, the electrons (Fermions) are assumed to fill all available states up to a certain energy (μ_F), with all states of energy greater than μ_F being completely empty. The velocity of the moving ion (V) is assumed to be considerably less than the maximum allowable electron velocity, v_F ($V << v_F$). Hence, for an electron-ion collision the velocity change suffered by the electron will be of the order of V (the maximum possible change will of course be 2V). Clearly, then, collisions for which the final

electron velocity lies inside the occupied zone of the electron momentum space will be forbidden by the Pauli principle. The only collisions allowed are those with electrons having a velocity differing from v_F by a value of the order of V. In momentum space the electrons occupy a volume of dimension $P_F = M\ v_F$, where M is the mass of an electron. The electrons capable of collision occupy a thin shell between P_F and $P_F + dP_F$ so that the volume formed by this shell will be approximately $P_F^2 dP_F$. Since the minimum volume in momentum space that can be occupied by a single electron is $\hbar^3$, the number of electrons engaging in collisions will be given by

$$n \approx \frac{P_F^2\ dP_F}{\hbar^3} \quad . \tag{24}$$

But by previous argument $dP_F \approx mV$ so that one has

$$n \approx \frac{M^3\ v_F^2\ V}{\hbar^3} \quad . \tag{25}$$

The interaction between the ion and the electron is basically Coulombic so the cross-section for collision, σ, will be proportional to the Rutherford scattering cross-section. Therefore

$$\sigma \approx \left(\frac{z\ e^2}{M\ v_F^2}\right)^2 \tag{26}$$

where z is the atomic number of the ion.

In this type of collision not forbidden by the Pauli principle the energy transferred during a collision, W, will be given by

$$W \approx \frac{1}{2} M \left[(v_F + V)^2 - v_F^2 \right]$$

$$\approx M v_F V \qquad (27)$$

to first order in V.

The total number of collisions taking place per unit time will be $n \sigma v_F$, and hence, the energy transfer per unit time will be $W n \sigma v_F$. Thus one has for the energy loss per unit time for the ion

$$- \frac{dW}{dt} = W n \sigma v_F \qquad (28)$$

$$\text{or,} \quad - \frac{dW}{dX} \frac{dX}{dt} = \frac{M^2 e^4}{\hbar^3} V^2 \quad . \qquad (29)$$

$$\text{Then,} \quad - \frac{dW}{dX} V = \frac{M^2 e^4}{\hbar^3} V^2 \quad . \qquad (30)$$

So, the energy loss per unit distance travelled by the ion is given by

$$- \frac{dW}{dX} \propto V \quad . \qquad (31)$$

For this very simple case, then, it has been shown that the stopping power due to electronic slowing

down is indeed proportional to the velocity of the ion. In actual fact, the process is very complicated and one is required to determine the probability that an electron will be captured and then lost by the moving ion. When the ion's velocity is much greater than the orbital velocities of the electrons its electrons are almost entirely stripped away upon entering slowing-down material. Initially, the ion loses energy by collisions with the electrons of the material which will not be retained by the ion because although there is a small, finite probability of capture of an electron during one collision there is a very much larger probability of its loss during the next collision. As the velocity of the ion decreases, however, to velocities of the order of the electron orbital velocity, the probability of electron loss decreases and that of electron capture increases until, finally, at ion velocities below the orbital velocity the loss probability approaches zero with a further increase in the capture probability. At this point an electron is captured and held by the ion in one of the lowest lying atomic shells. To capture a second electron in a higher shell (with a correspondingly lower orbital velocity than for the first shell) the ion must slow down to the next highest orbital velocity by the scattering process discussed above. Once the second electron is captured

a third may be captured (it will have a lower orbital velocity than either first or the second electron since it will be captured into a "higher" level than either of these) in a similar manner and so on for all the electrons (z) capable of being held by the ion, the only difference for each capture being the necessity of the ion to slow to the successively lower orbital velocities of these electrons within the ion.

At the point when the ion has slowed down to velocities less than the orbital velocity of the least tightly bound electron, the ion is mostly a neutral atom, and further energy loss proceeds predominantly by the elastic collisions of the screened electric fields of ion and stopping nuclei. The lower the velocity of the ion the more the latter process dominates, and the less is the energy loss to the orbital electrons. The final result is of course the stopping of the moving ion; that is, the thermalization of the ionic velocity.

Note that in the simple case considered the velocity of electrons above the conduction band, v_F, is approximately 8×10^8 cm/sec using Morse's expression (Mo 64) with $\rho = 10$ and that the velocity of electrons in the Bohr atom is 2.18×10^8 cm/sec. So the condition $V << v_F$ would indicate that at these velocities the ion would already have captured electrons into the lower

atomic shells before the simple case could even be considered. All this picture has shown is the approximate linear dependence of the stopping power on velocity, a fact which has experimentally been verified (Po 61), (Re 55), and (No 60).

Lindhard and Scharff (Li 61), (Li 63) have used the Thomas-Fermi statistical model of the atom to obtain a theoretical expression for the stopping power:

$$\frac{dE}{dX} = K \left(\frac{E}{M_1}\right)^{\frac{1}{2}} \qquad \text{KeV cm}^2/\text{mg} \qquad (32)$$

where E(v) is the energy of the moving ion, M_1 is its mass and

$$K = \frac{73.0\ z_1^{1/6}\ z_1\ z_2}{M_2 (z_1^{2/3} + z_2^{2/3})^{3/2}} \quad \text{for} \quad v \leqslant \frac{e^2}{\hbar}\ z_1^{2/3} \ . \qquad (33)$$

z_1 and z_2 are the atomic numbers of the moving ion and the stopping material atom respectively and M_2 is the mass of the stopping atom.

Firsov (Fi 58), (Fi 58), and (Fi 59) proposed an alternate method of deriving a theoretical approximation for the stopping power. He considered the regions of the interaction potentials of the two colliding ions to be defined by a surface S, so that the average effect of electrons crossing S from one region to another is that they assume the momentum of the atom in the latter region.

The energy loss of the electrons was given by Firsov as:

$$\xi = M \iint_S \frac{n\vec{v}}{4} \, d\vec{S} \, \dot{\vec{R}} d\vec{R} \tag{34}$$

where n and $\vec{v}$ are the number density and the velocity of the electrons respectively before crossing, $\vec{R}$ is the radial vector between the two nuclei, and $d\vec{S}$ is a surface element of S. $\vec{v}$ is then written in terms of n, n being written in terms of the potential ϕ by considering the Thomas-Fermi model of the atom. Therefore,

$$\xi = \frac{M^2 e^2}{4\pi^2 \hbar^3} \iint_S \phi^2 \, dS \, \dot{R} \, d \, R \quad . \tag{35}$$

The interaction potential was given by Firsov as:

$$\phi(r) = \frac{z_1 \, z_2 \, e^2}{r} \chi[\psi(z_1, \, z_2) \, \frac{r}{a}] \tag{36}$$

where $\chi(x)$ is the screening function in the Thomas-Fermi potential and where $a = a_o \ 0.8853 \ (z_1^{2/3} + z_2^{2/3})^{-\frac{1}{2}}$ is the screening length, a_o being the Bohr radius. The function $\psi = (z_1^{2/3} + z_2^{2/3})^{\frac{1}{2}}$ was assumed to be true over most of the range of the potential.

From these relations Firsov obtained

$$\frac{dE}{dX} = \frac{19.71 \ (z_1 + z_2)}{M_2} \left(\frac{E}{M_1}\right)^{\frac{1}{2}} \tag{37}$$

for the stopping power which, like Lindhard's formula and the very crude picture, predicts a linear velocity dependence.

These relations are only approximate, however, and represent a "smoothing" over all electron orbits. Using ion-gas (Mo 62), (Af 65), (Ev 65), (Ke 65) and ion-surface studies (Ra 64), (Da 65), (Pi 64), (Ro 65) it has been shown that the electron excitation losses occur in a step-wise fashion, the electrons being removed with discrete energies as a result of overlapping of successive energy levels. Indeed, the stopping power has been shown to be

$$\frac{dE}{dx} = c \left(\frac{E}{M_1}\right)^{S/2}$$

where $0.8 < S < 1.4$ (Ro 69), and c is a constant of proportionality.

1.4 Nuclear Stopping

In this stopping process momentum and kinetic energy are transferred to the translationary motion of the target atom as if it were a hard sphere (elastic collisions). Thus, the problem is much simpler than the electronic case where energy was transferred to the individual electrons of the target atom producing atomic excitation and ionization (inelastic collisions). The

scattering field, when screening is considered, leads to a potential of the incident particle of the form (Bo 48)

$$\phi(r) = \frac{z_1 z_2 e^2}{r} e^{-r/a} \qquad (39)$$

where r is the distance from the center of the atom, z_1e and z_2e are the charges of the incident and target particles respectively, and a is the screening length with $a = a_o S^{-1}$, a_o being the Bohr radius and S is the screening factor. For a single atom of charge ze, $S=z^{1/3}$ is an approximate estimate of the screening factor. In the case of a collision involving two atoms the two screening factors may be added in quadrature to obtain an approximate resultant factor S given by

$$S = \sqrt{S_1^2 + S_2^2} \qquad (40)$$

where $S_1 = z_1^{1/3}$ and $S_2 = z_2^{1/3}$ are the individual screening factors. S roughly accounts for the interaction of the two charge distributions corresponding to potentials of the type given by (39).

Define the quantity $\xi = b/a$, where $b \equiv 2|z_1 z_2 e^2|/(M_o v^2)$ is the collision parameter (b would be the minimum distance of approach for two repelling particles), $M_o = M_1 M_2/(M_1 + M_2)$ is the reduced mass of the system of two colliding particles of masses M_1 and M_2. The electron orbital speed of

the hydrogen atom is $v_o = e^2/\hbar$. Let λ be the wavelength of the particle of mass M_o and velocity v. Then,

$$\lambda = \frac{\hbar}{M_o v} \tag{41}$$

and if

$$\chi \equiv b/\lambda \quad ,$$

therefore,

$$\chi = \frac{2|z_1 z_2 e^2|}{\hbar v} = 2z_1 z_2 \frac{v_o}{v} \tag{42}$$

and

$$\xi = 2 z_1 z_2 S \frac{\mu}{M_o} \left(\frac{v_o}{v}\right)^2 \tag{43}$$

where μ is the mass of the electron.

Since $v_o = 2.18 \times 10^8$ cm/sec and since the maximum velocities that will be considered are $v \lesssim 10^8$ cm/sec and both particles are assumed to carry considerable charge ($z_1, z_2 \approx 25$) one always has the conditions that $\chi >> 1$ and $\xi << 1$. These conditions will remain over a considerable range of variation of the assumptions since the ratio μ/M_o will be of the order of 10^{-4}.

Consider now a particle passing through a layer of matter Δx in thickness with N atoms per unit volume (Bo 48). Further, it is assumed that Δx is small so that the initial velocity of the particle is not

appreciably changed upon its passage through the thickness. The number of collisions is then given by:

$$\omega = N \Delta x \sigma \tag{44}$$

where σ is the collision cross-section.

This frequency of collisions will fluctuate statistically and the probability of having n collisions in an interval of the momentum transfer T (from one particle to the other) will take on a Poisson distribution:

$$P(n) = \frac{\omega^n}{n!} e^{-\omega} \tag{45}$$

where the average number of collisions in the interval is ω.

In the i^{th} interval of the total collision process (formed by the successive collisions between the incident particle and the particles in the thickness Δx) with kinetic energy transfer T_i and number of collisions n_i (the average number being ω_i) the energy loss is given by

$$\Delta E_i = n_i T_i \tag{46}$$

and, over all intervals one has that

$$\Delta E = \sum_i n_i T_i \quad . \tag{47}$$

Replacing n_i with its mean value gives an average energy loss

$$\overline{\Delta E} = \sum_i T_i \omega_i \quad . \tag{48}$$

If these intervals are made infinitesimally small the summation becomes an integral so that

$$\overline{\Delta E} = \int T \, d\omega = N \Delta x \int T \, d\sigma \tag{49}$$

Δx being a constant element of the total range R.

$d\sigma$ may be evaluated very easily by considering the simple case of a Rutherford type of collision:

$$d\sigma = \left(\frac{z_1 z_2 e^2}{2 M_o v^2}\right) \frac{d\Omega}{\sin^4 \frac{\theta}{2}} \tag{50}$$

where $d\Omega = 2\pi \sin \theta \, d\theta$ is the solid angle, θ is the deflection suffered by the incident particle in the center of mass system (figure 3a), M_o is the reduced mass defined above, and v is the initial velocity of the incident particle.

From the kinematics of the collision the kinetic energy transferred during a single collision is given by

$$T = T_M \sin^2 \frac{\theta}{2} \tag{51}$$

where

$$T_M = \frac{2 M_o^2}{M_2} v^2 = \frac{4 M_1 M_2}{(M_1 + M_2)^2} E$$

Figure 3a. The collision between particle 1 moving from the left with initial velocity $\vec{v}$ (in lab system with particle 2 initially at rest) and particle 2 moving from the right with the velocity of the center of mass $\vec{v}_c$ is shown. Particles 1 and 2 are scattered through an angle θ in the center of mass system and particle 2 is scattered through angle θ_2 in lab system acquiring energy T. Equation 51 follows immediately from this diagram.

Figure 3b. Hyperbolic orbits of particles 1 and 2 in the center of mass system are shown with the asymptotic angles α. F is the focus of orbit 1 and $\vec{r}$ is the vector joining the focus with particle 1 and makes an angle θ' with the vertical symmetry axis. The impact parameter P is shown.

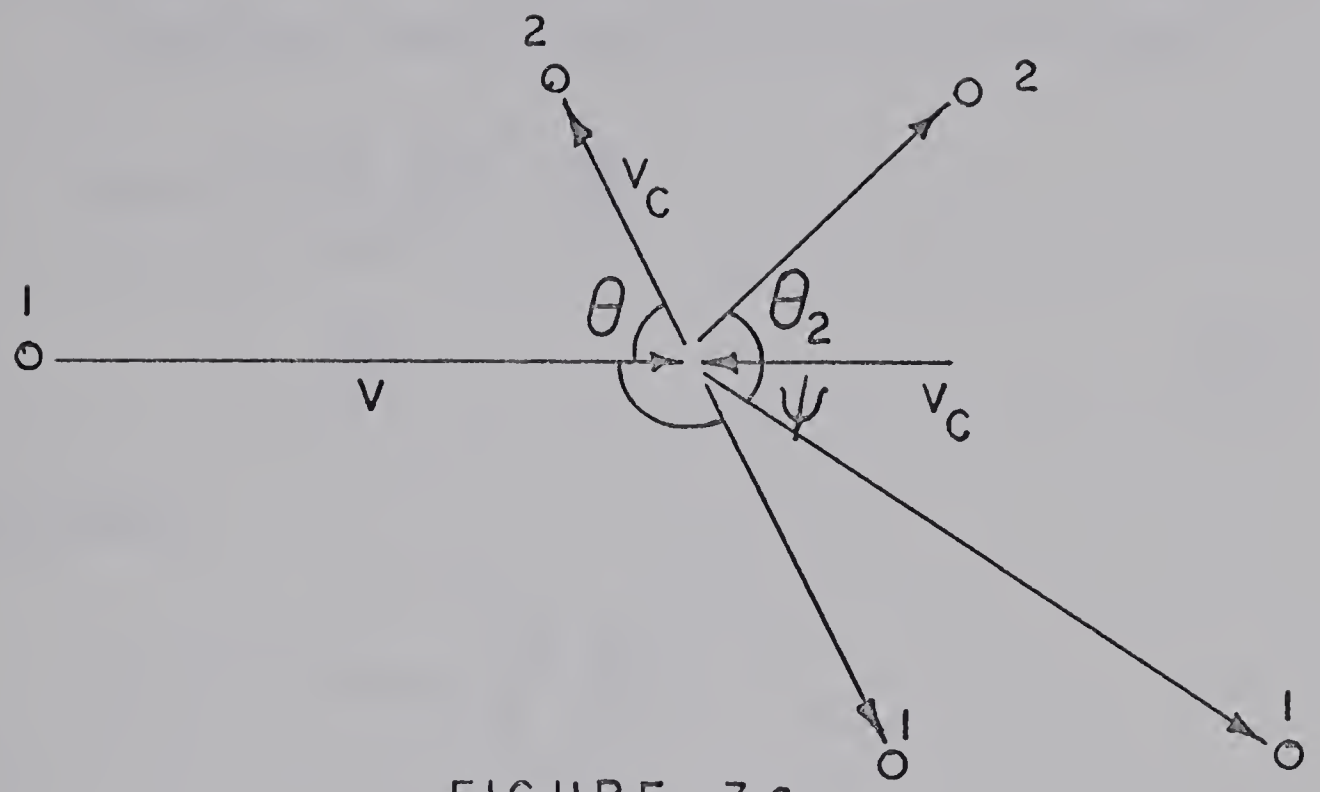

FIGURE 3a

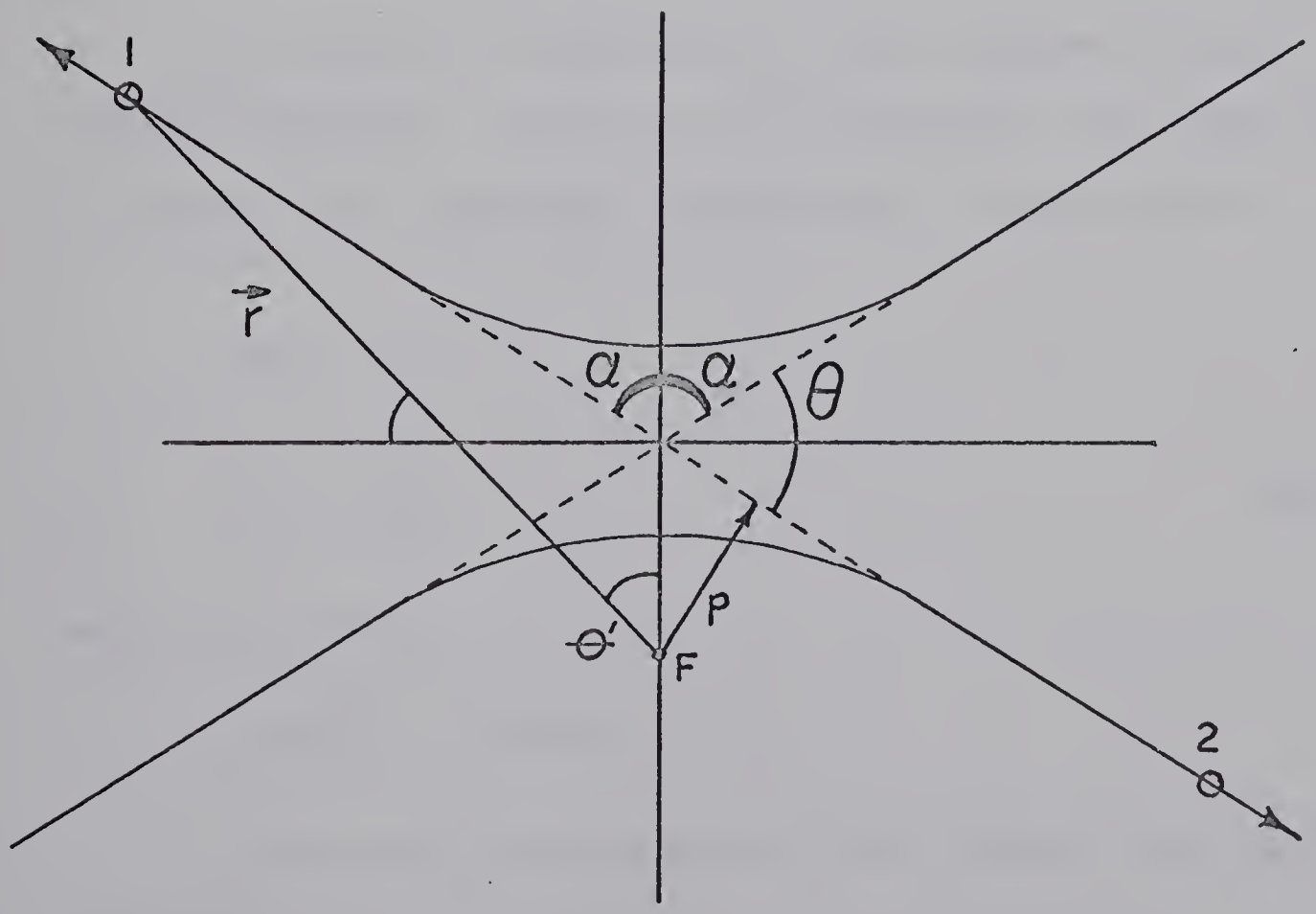

FIGURE 3b

is the maximum kinetic energy transfer and $E = \frac{1}{2} M_1 v^2$.

Therefore substituting (51) into (50) gives

$$d\sigma = \frac{2\pi z_1^2 z_2^2 e^4}{M_2 v^2} \frac{dT}{T^2}$$

$$= B_n \frac{dT}{T^2} \qquad (52)$$

and hence,

$$\overline{\Delta E} = N \Delta x B_n \int_{T_a}^{T_M} \frac{dT}{T}$$

$$= N \Delta x B_n \log \frac{T_M}{T_a} \quad . \qquad (53)$$

In order to evaluate T_a, the minimum kinetic energy transfer, consider the scattering case depicted in figure 3b. From the diagram one can see that

$$2\alpha + \theta = \pi$$

or $$\frac{\theta}{2} = \frac{\pi}{2} - \alpha \qquad (54)$$

and, therefore

$$\tan \frac{\theta}{2} = \cot \alpha.$$

Now from the solution of the orbital equation (Sy 64)

$$\frac{d^2u}{d\theta^2} + u = -\frac{M_o K}{L^2} \tag{55}$$

one has

$$u \equiv \frac{1}{r} = B + A \cos(\theta - \theta_o) \tag{56}$$

where $K = z_1 z_2 e^2$, L is the orbital angular momentum, and $B = -M_o K/L^2$. Define

$$\varepsilon \equiv A/|B|$$

which is the eccentricity of the orbit, and

$$a \equiv \left|\frac{B}{A^2 - B^2}\right|$$

one finds, then

$$r = \frac{a(\varepsilon^2 - 1)}{\varepsilon \cos\theta - 1} \tag{57}$$

so that $r \to \infty$ $(\theta \to \alpha)$ for $\cos\alpha = 1/\varepsilon$ or,

$$\cot\alpha = (\varepsilon^2 - 1)^{-\frac{1}{2}} \tag{58}$$

which, by evaluating A from the initial conditions of the orbit and thus finding that

$$\varepsilon = \left(1 + \frac{2 E L^2}{M_o K^2}\right) \tag{59}$$

becomes

$$\tan \frac{\theta}{2} = \cot \alpha = (\varepsilon^2 - 1)^{-\frac{1}{2}} = \left(\frac{M_o K^2}{2 E L^2}\right)^{\frac{1}{2}}, \qquad (60)$$

since it is assumed that momentum is conserved $L = M_o v P$, giving the result (P is defined in figure 3b)

$$\tan \frac{\theta}{2} = \frac{z_1 z_2 e^2}{M_o v^2} \frac{1}{P} = \frac{1}{2} \frac{b}{P} \qquad (61)$$

one should observe that for p small compared to a, collisions will occur only in the unscreened part of the field. Therefore, the minimum angle θ_a will be given by

$$\tan \frac{\theta_a}{2} = \frac{b}{2a} = \frac{\xi}{2} \approx \frac{\theta_a}{2} \quad . \qquad (62)$$

It is permissible to accept only first order terms in $\frac{\theta_a}{2}$ since the condition $\xi << 1$ holds.

However since

$$T_a = T_M \sin^2 \frac{\theta_a}{2} \approx T_M \left(\frac{\theta_a}{2}\right)^2 \qquad (63)$$

then,

$$\frac{T_M}{T_a} = \left(\frac{\theta_a}{2}\right)^{-2} = \left(\frac{\xi}{2}\right)^{-2}$$

$$= \left[\frac{2 E M_2 \hbar^2}{(M_1+M_2) z_1 z_2 e^4 \mu (z_1^{2/3} + z_2^{2/3})^{\frac{1}{2}}}\right]^2 . \qquad (64)$$

Therefore one has for the nuclear stopping power upon combining (53) and (64)

$$\frac{\overline{\Delta E}}{\Delta x} = N B_n' \log \left[\frac{2 E M_2 \hbar^2}{(M_1+M_2) z_1 z_2 e^4 \mu (z_1^{2/3} + z_2^{2/3})^{\frac{1}{2}}} \right] \qquad (65)$$

where

$$B_n' = \frac{2\pi z_1^2 z_2^2 M_1 e^4}{M_2 E} \quad . \qquad (66)$$

Lindhard and Scharff have introduced the dimensionless variables

$$\rho = \frac{4\pi N M_2 a^2 M_1}{(M_1 + M_2)^2} x \qquad (67)$$

and

$$\varepsilon = \frac{a M_2}{z_1 z_2 e^2 (M_1 + M_2)} E \qquad (68)$$

with

$$a = \frac{0.8853 \hbar^2}{(z_1^{2/3} + z_2^{2/3})^{\frac{1}{2}} \mu e^2} \quad . \qquad (69)$$

Using these variables (65) becomes

$$\frac{d\varepsilon}{d\rho} = \frac{1}{2\varepsilon} \log (2.259 \varepsilon) \quad . \qquad (70)$$

According to Robertson (Ro 69) in his evaluation of $F(\tau)$, the nuclear stopping formula due to Lindhard

(72) can be approximated by the following functions:

$$\frac{d\varepsilon}{d\rho} = 1.97\ \varepsilon^{\frac{1}{2}} \exp(-1.82\ \varepsilon^{\frac{1}{2}}) + 0.025\ \varepsilon^{\frac{1}{2}}$$

$$\text{for} \quad \varepsilon < 14 \ ,$$

$$\frac{d\varepsilon}{d\rho} = \frac{1}{4} \left\{ \frac{(\varepsilon - 14) \log (2.259\ \varepsilon)}{2\varepsilon} \right.$$

$$+ (18 - \varepsilon)(1.97\ \varepsilon^{\frac{1}{2}} \exp (-1.82\ \varepsilon^{\frac{1}{2}})$$

$$\left. + 0.0225\ \varepsilon^{\frac{1}{2}} \right\} \ , \qquad \text{for } 14 \leqslant \varepsilon \leqslant 18$$

$$\frac{d\varepsilon}{d\rho} = \frac{1}{2\varepsilon} \log (2.259\ \varepsilon) \qquad \text{for} \quad \varepsilon > 18$$

so, from the last relation one sees that both the approximation and the Lindhard stopping formula join smoothly with the Rutherford stopping in the high energy region. The above functions agree with (72) to within 20% over the range of ε considered.

1.5 $F(\tau)$ Calculation of Blaugrund (Bl 66)

Upon examining the behavior of the recoil ions in a stopping material it has been seen that the two main processes of energy loss are electronic and atomic collisions, and that atomic collisions can be further divided into kinetic energy losses and atomic scattering.

The previous discussions have provided enough information to determine v(t), the speed of the recoil ion in the stopping material, but in order to evaluate (17) it is necessary to include the effects of scattering which results in the $\overline{\cos \phi(t)}$ term in the expression for $F(\tau)$.

Lindhard and Scharff (Li 63) derive a screened potential $\phi(r)$ by an extrapolated perturbation method for classical scattering, and from this obtain an expression for the atomic scattering cross-section:

$$d\sigma = \pi a^2 \frac{dt}{2t^{3/2}} f(t^{\frac{1}{2}}) \qquad (71)$$

where $t^{\frac{1}{2}} = \varepsilon \sin \frac{\theta}{2}$, ε being the dimensionless quantity given by (68), and as before $\sin^2 \frac{\theta}{2} = T/T_M$. $f(t^{\frac{1}{2}})$ is called the universal differential scattering cross-section for elastic nuclear collisions and the behavior of this function is shown in figure 2 of Lindhard's paper (Li 63) and is derived using a Thomas-Fermi potential.

It follows from the above definitions that t/ε is the dimensionless kinetic energy and using the expression $d\sigma/\pi a^2$ as the dimensionless cross-section (49) becomes

$$\left(\frac{d\varepsilon}{d\rho}\right)_n = \frac{1}{\pi a^2} \int_0^{\varepsilon} \frac{t}{\varepsilon} d\sigma \ (t^{\frac{1}{2}})$$

$$= \frac{1}{\varepsilon} \int_0^{\varepsilon} f(x)\, dx \qquad (72)$$

using (71), where $x = t^{\frac{1}{2}}$.

From before for the low ion velocity range ($v \lesssim \frac{e^2}{h} z_1^{2/3}$) the electronic stopping power can be written in dimensionless units as

$$\left(\frac{d\varepsilon}{d\rho}\right)_e = k\, \varepsilon^{\frac{1}{2}} \tag{73}$$

where

$$k = z_1^{1/6} \frac{0.0793\, z_1^{\frac{1}{2}} z_2^{\frac{1}{2}} (A_1 + A_2)^{3/2}}{(z_1^{2/3} + z_2^{2/3})^{3/4} A_1^{3/2} A_2^{\frac{1}{2}}} \quad .$$

Two new parameters are introduced:

$\tilde{v} \equiv \frac{hc}{e^2} \frac{v}{c}$ is the dimensionless velocity of the ion, and $\mathcal{M}$ is defined by the relation $\varepsilon = \frac{1}{2} \mathcal{M} \tilde{v}^2$, so that

$$\mathcal{M} = \frac{1.63 \times 10^3 A_1 A_2}{z_1 z_2 (z_1^{2/3} + z_2^{2/3})^{\frac{1}{2}} (A_1 + A_2)} \quad . \tag{74}$$

One can also define a dimensionless time variable, θ, such that:

$$\frac{d\rho}{d\theta} = \tilde{v} \quad . \tag{75}$$

Thus, one has $\theta = t/T$ where t is time in seconds and the coefficient T is given by

$$T = \frac{\hbar\ (A_1 + A_2)^2}{e^2\ 4\pi a^2\ N\ A_1\ A_2} \quad . \tag{76}$$

Using these expressions the integral (20) becomes

$$\theta = (\tfrac{1}{2}\mu\ell)^{\frac{1}{2}} \int_{\varepsilon}^{\varepsilon_o} \frac{d\varepsilon}{\varepsilon^{\frac{1}{2}} \frac{d\varepsilon}{d\rho}} \tag{77}$$

where $d\varepsilon/d\rho = (d\varepsilon/d\rho)_n + (d\varepsilon/d\rho)_e$ and ε_o is the energy of the moving ion at t=0. This integration may be performed numerically to give $\tilde{v}$ as a function of θ. Having defined these quantities, $\overline{\cos\ \phi}$, the average projection of the velocity onto the initial beam direction, may now be evaluated.

Lewis (Le 50) has given the angular distribution for an initially collimated beam of ions after passing through a distance, x, of a stopping material:

$$F(\phi,x) = \frac{1}{4\pi} \sum_{\ell=0}^{\infty} (2\ell+1)\ P_\ell(\cos\ \phi)\ \exp\left(-\int_0^x K_{\ell\phi}\, dx\right) \tag{78}$$

where

$$K_{\ell\phi} = N \int [1 - P_\ell(\cos\ \phi)]\ d\sigma(\phi)\ , \tag{79}$$

N being the number density of stopping atoms and $d\sigma(\phi) = \sigma(\phi)\ d\Omega_\phi$ is the differential cross-section as a function of the lab angle, ϕ. $P_\ell(\cos\ \phi)$ are the unnormalized Legendre polynomials. (For an outline of the derivation of (78) see appendix 1).

From (78) one gets immediately,

$$\overline{P_n(\cos\phi)} = \int F(\phi,x)\, P_n(\cos\phi)\, d\hat{\phi}\, d\theta$$

$$= \frac{2\ell+1}{4\pi} \int_0^{2\pi} \int_{-1}^{1} P_n^2(\cos\phi)\, d(\cos\phi)\, d\theta$$

$$\times \exp\left(-\int_0^x K_{n\phi}\, dx\right)$$

$$= \exp\left(-\int_0^x K_{n\phi}\, dx\right) \qquad (80)$$

or, for n = 1

$$\overline{\cos\phi} = \exp\left(-\int_0^x K_{1\phi}\, dx\right) . \qquad (81)$$

One also has the well-known expression relating the lab angles to the center of mass angles ϕ and Θ respectively:

$$\tan\phi = \frac{\sin\Theta}{r + \cos\Theta} \qquad (82)$$

where $r = A_1/A_2$, A_1 being the mass of the recoil ion and A_2 that of the stopping ion.

Solving (82) for cos ϕ one finds

$$\cos\phi = \frac{r + \cos\Theta}{(r^2 + 2r\cos\Theta + 1)^{\frac{1}{2}}} \qquad (83)$$

which, when expanded in terms of Legendre polynomials (see appendix 2) becomes

$$\cos\phi = \begin{cases} P_1(\cos\theta) + \sum_{n=1}^{\infty} (-1)^n \frac{n+1}{2n+1}[P_{n+1}(\cos\theta) - P_{n-1}(\cos\theta)]r^n \\ \qquad\qquad \text{for } r < 1 \qquad\qquad (84a) \\ 1 + \sum_{n=1}^{\infty} (-1)^n \frac{n}{2n+1}[P_{n+1}(\cos\theta) - P_{n-1}(\cos\theta)]r^{-(n+1)} \\ \qquad\qquad \text{for } r > 1 \qquad\qquad (84b) \end{cases}$$

In expression (80)

$$K_{\ell\phi} = N \int [1 - P_\ell(\cos\phi)]\, d\sigma(\phi) \quad .$$

Putting the expression for $\cos\phi$ into $k_{1\phi}$ one gets

$$K_{1\theta} = N \int [1 - \cos\phi(\theta)]\, d\sigma(\theta) \qquad (85)$$

$$= N \int [1 - P_1(\cos\theta)] + \sum_{n=1}^{\infty} (-1)^n \frac{n+1}{2n+1} r^n$$

$$\times [-P_{n+1}(\cos\theta) + P_{n-1}(\cos\theta)]d\sigma(\theta), \qquad (86)$$

using (84a) and using $d\sigma(\theta)$ instead of $d\sigma(\phi)$ in (79).

The first square-bracketed term in (86) is immediately seen to be $k_{1\theta}$, where

$$k_{1\theta} = N \int [1 - P_1(\cos\theta)]\, d\sigma(\theta) \quad . \qquad (87)$$

The second bracketed term may be rewritten in the form,

$$[1 - P_{n+1}(\cos\theta)] - [1 - P_{n-1}(\cos\theta)], \qquad (88)$$

so that now these two terms taken into the integration become

$$\sum_{n=1}^{\infty} (-1)^n \frac{n+1}{2n+1} r^n (k_{n+1\theta} - k_{n-1\theta}) \quad . \qquad (89)$$

Then,

$$\overline{\cos\phi} = \exp(-\int_0^x k_{1\theta} dx).\exp(-\int_0^x (-1)^n \frac{n+1}{2n+1} r^n \times [k_{n+1\theta} - k_{n-1\theta}]) \qquad (90)$$

$$= \overline{P_1(\cos\theta)} \prod_{n=1}^{\infty} \left[\frac{\overline{P_{n+1}(\cos\theta)}}{\overline{P_{n-1}(\cos\theta)}}\right] (-1)^n (\frac{n+1}{2n+1}) r^n$$

$$r < 1 \qquad (91)$$

Similarly for $r > 1$

$$\overline{\cos\phi} = \prod_{n=1}^{\infty} \left[\frac{\overline{P_{n+1}(\cos\theta)}}{\overline{P_{n-1}(\cos\theta)}}\right] (-1)^{n+1} \frac{n}{2n+1} \frac{1}{r^{n+1}}$$

using the properties of the exponential function and the relation

$$\overline{P_n(\cos\,\theta)} = \exp\left(-\int_0^x k_{n\theta}\,dx\right) .$$

In order to calculate the $P_\ell(\cos\,\theta)$ terms it will be necessary to calculate $\overline{\cos\,\theta}$, which is given by (81) and (79) upon replacing ϕ with θ and setting $\ell = 1$. The integrand of (79) can be written as

$$(1 - \cos\,\theta) = 2\,\sin^2\frac{\theta}{2} \quad . \tag{92}$$

From before we have

$$d\sigma(\theta) = \pi a^2\,\frac{dt}{2t^{3/2}}\,f(t^{\frac{1}{2}})$$

where $t^{\frac{1}{2}} = \varepsilon\,\sin\frac{\theta}{2}$.

$$d\sigma(\theta) = \pi a^2\,\frac{d(t^{\frac{1}{2}})}{\varepsilon^2\,\sin^2\frac{\theta}{2}}\,f(t^{\frac{1}{2}})$$

$$= \pi a^2\,\frac{dy}{\varepsilon^2\,\sin^2\frac{\theta}{2}}\,f(y)\ , \quad y \equiv t^{\frac{1}{2}} \tag{93}$$

Therefore

$$[1 - \cos\,\theta]\,d\sigma(\theta) = \frac{2\pi a^2}{\varepsilon^2}\,f(y)\,dy$$

giving

$$K_{1\theta} = \frac{2\pi N a^2}{\varepsilon}\,\left(\frac{d\varepsilon}{d\rho}\right)_n \tag{94}$$

by using (79) and since

$$\left(\frac{d\varepsilon}{d\rho}\right)_n = \frac{1}{\varepsilon} \int_0^{\varepsilon} f(y)\, dy \qquad (72)$$

which is, in fact, an average of f(y) and thus is assumed to be a constant.

Examining the integration over x in (81) recall the previous definition of ρ; so one may write

$$x = \frac{1}{4\pi Na^2} \frac{(A_1 + A_2)^2}{A_1 A_2} \rho = \frac{1}{4\pi Na^2} \frac{(r+1)^2}{r} \rho \quad . \qquad (95)$$

Thus $dx \propto d\rho = d\varepsilon/\left(\frac{d\varepsilon}{d\rho}\right)$. Hence,

$$\int_0^x K_{1\theta}\, dx = \int_{\varepsilon}^{\varepsilon_o} \frac{2\pi Na^2}{\varepsilon} \frac{(d\varepsilon/d\rho)_n}{d\varepsilon/d\rho} \frac{1}{4\pi Na^2} \frac{(r+1)^2}{r}\, d\varepsilon$$

$$= \frac{1}{2} \frac{(r+1)^2}{r} \int_{\varepsilon}^{\varepsilon_o} \frac{(d\varepsilon/d\rho)_n}{\varepsilon(d\varepsilon/d\rho)}\, d\varepsilon \equiv \frac{1}{2} \frac{(r+1)^2}{r} I \qquad (96)$$

where

$$I \equiv \int_{\varepsilon}^{\varepsilon_o} \frac{(d\varepsilon/d\rho)_n}{\varepsilon(d\varepsilon/d\rho)}\, d\varepsilon \quad .$$

Therefore,

$$\overline{\cos \phi} = \exp\left[-\frac{1}{2} \frac{(1+r)^2}{r} I\right] \quad . \qquad (97)$$

For the case r = 1 one has $\phi = \frac{1}{2}\theta$ and $\overline{\cos \phi}$ may, in principle, be calculated directly without any approximations. Using the approximation,

$$\overline{P_\ell(\cos\Theta)} \approx \overline{(\cos\Theta)^\ell} \tag{98}$$

one has for $r \neq 1$

$$\overline{\cos\phi} = \begin{cases} \overline{\cos\Theta} \prod_{n=1}^{\infty} \overline{[\cos\Theta]}^{(-1)^n \frac{2(n+1)}{2n+1} r^n}, & r < 1 \qquad (99a) \\ \prod_{n=1}^{\infty} \overline{[\cos\Theta]}^{(-1)^{n+1} \frac{2n}{2n+1} \frac{1}{r^{n+1}}}, & r > 1 \qquad (99b) \end{cases}$$

Or, putting in (97) one has

$$\overline{\cos\phi} = \exp\left\{-\frac{1}{2}\frac{1}{r} I\left[(1+2r+r^2)\left(\sum_n (-1)^n r^n \frac{2(n+1)}{2n+1} + 1\right)\right]\right. . \tag{100}$$

The square bracketed term, upon multiplying the factors, becomes

$$\sum_n \left((-1)^n \frac{2(n+1)}{2n+1} r^n + (-1)^n \frac{4(n+1)r^{n+1}}{2n+1} + (-1)^n \frac{2(n+1)}{2n+1} r^{n+2}\right)$$

$$+ r^2 + 2r + 1 .$$

Since n is a dummy index one can change n to n-1 and n to n-2 in the second and third terms respectively to reduce the sum to common powers of r. Thus, one has

$$\sum_{n=1} (-r)^n \frac{2(n+1)}{2n+1} - \sum_{n=2} \frac{4n(-r)^n}{2n-1} + \sum_{n=3} (-r)^n \frac{2(n-1)}{2n-3} + 1 + 2r + r^2$$

$$= 1 + \frac{2r}{3} - \frac{7}{15} r^2 + 8 \sum_{n=3}^{\infty} (-r)^n \frac{1}{(2n+1)(2n-1)(2n-3)}$$

$$\equiv G(r) \qquad \text{for} \qquad r < 1 \qquad (101a)$$

and similarly, for $r > 1$ one has

$$G(r) = \frac{2}{3} + \frac{8}{15} \frac{1}{r} - 8 \sum_{n=3}^{\infty} \frac{(-1/r)^{n-1}}{(2n+1)(2n-1)(2n-3)} \qquad (101b)$$

so that

$$\overline{\cos \phi} = \exp \left[- \frac{1}{2} \frac{1}{r} G(r) \; I \right] \quad . \qquad (102)$$

Since the summation will be proportional to n^{-3}, it may be neglected for $r < 1$, and even for $r \approx 1$.

From a plot of $(d\varepsilon/d\rho)_n$ it can be seen (Bl 66) that the curve may be approximated by $(d\varepsilon/d\rho)_n = 0.4\ \varepsilon^{-\frac{1}{2}}$ for the range $1.2 < \varepsilon < 20$. Thus, the stopping power becomes

$$\frac{d\varepsilon}{d\rho} = 0.4\ \varepsilon^{-\frac{1}{2}} + k\ \varepsilon^{\frac{1}{2}} \qquad (103)$$

using (23) and (73); and putting these into (77) and the definition for I, one finds

$$\theta = (\tfrac{1}{2}m)^{\frac{1}{2}} \int_{\varepsilon}^{\varepsilon_o} \frac{d\varepsilon}{0.4 + k\varepsilon}$$

$$= -(\tfrac{1}{2}m)^{\frac{1}{2}} \frac{1}{k} \log \left(\frac{1 + 0.4/k\varepsilon}{1 + 0.4/k\varepsilon_o}\right) \qquad (104)$$

or

$$\frac{\varepsilon}{\varepsilon_o} \frac{1 + 0.4/k\varepsilon}{1 + 0.4/k\varepsilon_o} = \exp\left(-\sqrt{\frac{2}{m}}\, k\theta\right) \qquad (105)$$

and

$$I = 0.4 \int_{\varepsilon}^{\varepsilon_o} \frac{d\varepsilon}{(0.4 + k\varepsilon)\varepsilon}$$

$$= \log \left(\frac{1 + 0.4/k\varepsilon_o}{1 + 0.4/k\varepsilon}\right)^{-1} \qquad (106)$$

so that

$$\overline{\cos\ \phi} = \left[\frac{1 + 0.4/k\varepsilon}{1 + 0.4/k\varepsilon_o}\right]^{-\frac{1}{2}rG} . \qquad (107)$$

Now, both expressions (105) and (107) may be evaluated numerically without much difficulty.

Thus, one has both v (or ε) and $\overline{\cos\ \phi}$ as functions of time, θ, and attention can now be returned to the calculation of $F(\tau)$. Recall that

$$\frac{\overline{\Delta E_\gamma}}{\Delta E_{\gamma o}} = F(\tau) = \frac{\int_0^\infty v(t)\ \overline{\cos\ \phi(t)}\ \exp(-t/\tau)dt}{\int_0^\infty v_o \exp(-t/\tau)dt}$$

$$= \frac{T}{\tau} \int_0^\infty \frac{\tilde{v}(\theta)}{\tilde{v}_o}\ \overline{\cos\ \phi(\theta)}\ \exp\left(-\frac{\theta}{\tau/T}\right)d\theta \qquad (108)$$

using the variables $\theta = t/T$ and $\tilde{v} = \frac{\hbar c}{e^2} v$. A remark should be made here that $\overline{v \cos \phi}$ should actually be used. However, the corrections to I from the use of $v \overline{\cos \phi}$ is only 5% to 10% (Bl 66) for $r = 1$ and $(\frac{d\varepsilon}{d\rho})_n >> (\frac{d\varepsilon}{d\rho})_e$, and much less for all other cases.

For very short lifetimes ($\overline{\Delta E_\gamma} \approx \Delta E_{\gamma o}$ and $T << \alpha \equiv (2)^{\frac{1}{2}} T/k$) a small quantity $\tilde{F}(\tau)$ is defined such that

$$\tilde{F}(\tau) = \frac{\Delta E_{\gamma o} - \overline{\Delta E_\gamma}}{\Delta E_{\gamma o}}$$

$$= \frac{t}{\tau} \int_0^\infty (1 - \frac{\tilde{v}}{\tilde{v}_o} \overline{\cos \phi}) \exp(- \frac{\theta}{\tau/T}) d\theta. \quad (109)$$

Consider, now, the case where electronic stopping dominates $[(d\varepsilon/d\rho)_e >> (d\varepsilon/d\rho)_n$ for $\theta \lesssim \tau/T]$. Assume that

$$\frac{1}{r} \exp (\frac{2T}{\alpha}) \quad 0.4/k\varepsilon_o << 1$$

which, in most experimental situations, is equivalent to saying that

$$\frac{0.4}{k\varepsilon_o} \equiv d_o << 1$$

with

$$d \equiv \frac{0.4}{k\varepsilon} \quad .$$

Thus, from (105) one finds

$$\frac{1}{d} = \frac{1}{d_o} \; e^{-x} \; [e^{-x} - 2d_o \sinh x] \tag{110}$$

where $x = \theta T/\alpha$, or

$$d \approx d_o \; e^{2x} \; [1 + 2d_o \; e^{x} \sinh x] \tag{111}$$

to first order in d_o. Note also that

$$\frac{\tilde{v}}{\tilde{v}_o} = \left(\frac{d_o}{d}\right)^{\frac{1}{2}} \approx e^{-x} \; [1 - d_o \; e^{x} \sinh x] \; . \tag{112}$$

From (107) it can be seen that

$$\overline{\cos \phi} \; = \; \left[\frac{1 + d}{1 + d_o}\right]^{-n} \tag{113}$$

where $n = \frac{1}{2r} G$. Or,

$$\overline{\cos \phi} \approx 1 + n \, d_o - n \, d \quad , \tag{114}$$

to first order in d_o and d, so that

$$\frac{\tilde{v}}{\tilde{v}_o} \; \overline{\cos \phi} \approx e^{-x} - d_o \sinh x + n \, d_o \, e^{-x} - n \, d_o \, e^{x}. \tag{115}$$

Or,

$$\frac{\tilde{v}}{\tilde{v}_o} \; \overline{\cos \phi} \approx e^{-\frac{T}{\alpha}\theta} - \frac{0.4}{k\varepsilon_o} \left[1 + \frac{1}{r} G\right] \sinh \left(\frac{T}{\alpha} \theta\right) \; . \tag{116}$$

Putting this into expression (108) for $F(\tau)$ and carrying out the trivial integration one finds

$$F(\tau) = \frac{1}{1 + \tau/\alpha} - \frac{0.4}{k\varepsilon_o}\left(1 + \frac{1}{r} G\right) \frac{\tau/\alpha}{1 - (\tau/\alpha)^2} \quad . \qquad (117)$$

The first term of (117) is due to electronic stopping and the second is due to nuclear stopping, which itself is composed of two parts: loss of kinetic energy by the moving ion to the surrounding nuclei in the collision, and scattering (change in direction) of the moving ion. Since G is of the order of unity, one can easily see that the scattering term dominates for r much less than unity, which corresponds to the case of light ions slowing down in a high mass number backing. The above expression holds for the range $\tau/\alpha \lesssim 0.3$ to 0.5.

In this derivation it has been assumed that the stopping material is composed of atoms of only one z and A ignoring the fact that many materials available are composites of several types of atoms. If m, z_2, A_2 refer to the heaviest stopping atom and m_i, z_{2i}, A_{2i} refer to the i^{th} lighter atoms then (77) becomes (Bl 66)

$$\theta = \left(\frac{1}{2}m\right)^{\frac{1}{2}} \int_{\varepsilon}^{\varepsilon_o} \frac{d\varepsilon}{\varepsilon^{\frac{1}{2}}\left[\frac{d\varepsilon}{d\rho} + \sum_i C_i \left(\frac{d\varepsilon}{d\rho}\right)_i\right]} \qquad (118)$$

where θ and ε pertain to the heaviest scattering atom and

$$C_i = \frac{N_i}{N} \frac{z_{2i}}{z_2} \frac{a_i}{a} \frac{A_1 + A_2}{A_1 + A_{2i}} \tag{119}$$

and where $(\frac{d\varepsilon}{d\rho})_i$ is the total specific stopping power at an energy $(m_i/m)\varepsilon$.

For I one has, now,

$$I = \int_{\varepsilon}^{\varepsilon_o} \frac{(\frac{d\varepsilon}{d\rho})_n + \sum_i C_i \frac{A_{2i}}{A_2} \frac{G_i}{G} (\frac{d\varepsilon}{d\rho})_{ni}}{\varepsilon[\frac{d\varepsilon}{d\rho} + \sum_i C_i (\frac{d\varepsilon}{d\rho})_i]} d\varepsilon \tag{120}$$

and

$$\overline{\cos \phi} = \left[\frac{1 + d_n/d_e\varepsilon}{1 + d_n/d_e\varepsilon_o}\right] - \frac{G}{2r} \frac{d_n'}{d_n} \tag{121}$$

where,

$$d_e = k + \sum_i C_i k_i (m_i/m)^{\frac{1}{2}}$$

$$d_n = 0.4 \left[1 + \sum_i C_i (m/m_i)^{\frac{1}{2}}\right]$$

$$d_n' = 0.4 \left[1 + \sum_i C_i \frac{A_{2i}}{A_2} \frac{G_i}{G} (\frac{m}{m_i})^{\frac{1}{2}}\right] .$$

Then,

$$F(\tau) \approx \frac{1}{1 + \tau/\alpha} - \frac{d_n}{d_e\varepsilon_o} (1 + \frac{A_2}{A_1} G \frac{d_n'}{d_n}) \frac{\tau/\alpha}{1 - (\tau/\alpha)^2} . \tag{122}$$

Since the stopping process is purely an atomic effect, having nothing to do with molecular bonding, the resultant stopping power of a molecule is proportional to the sum of the stopping powers due to the individual atoms of the molecule. Thus, for a compound consisting of molecules of n_i atoms of type i, the stopping power is given by

$$\left(\frac{dE}{dx}\right)_{molec.} = \frac{\sum_i n_i M_i \left(\frac{dE}{dx}\right)_i}{\sum_i n_i M_i} \quad , \qquad (123)$$

so, clearly, for a molecule consisting of a heavy and light atom, the greatest contribution to the stopping will come from the heavy atom.

It has been shown previously that where large angle scattering is negligible ($\frac{d_n}{d_e \varepsilon} << 1$, $\tau/\alpha < 1$) electronic stopping dominates and that this should be proportional to the velocity of the ion:

$$\left(\frac{dE}{dx}\right)_e \equiv \frac{dE}{dx} = k\, v(t) \qquad (124)$$

where k is a constant of proportionality.

One notes that

$$\frac{dE}{dx} = \left(\frac{dE}{dt}\right)/\left(\frac{dx}{dt}\right) = M_1\, v\left(\frac{dv}{dt}\right)/v = M_1 \frac{dv(t)}{dt} \quad . \qquad (125)$$

Therefore by combining (125) and (124), and integrating one has that

$$v = v_o \exp\left(-\frac{k}{M_1} t\right) \tag{126}$$

where v_o is the initial speed of the ion.

Define a parameter α such that

$$M_1/\alpha \equiv k$$

or, in dimensionless variables

$$\alpha \equiv (2\mathcal{M})^{\frac{1}{2}} T/k$$

which is known as the characteristic electronic slowing down time.

Ignoring the scattering term $\overline{\cos \phi}$ in (17) one has

$$F(\tau) = \frac{1}{v_o} \int_0^\infty v_o \exp(-t/\alpha) \exp(-t/\tau)\, dt$$

$$= \frac{1}{1 + \tau/\alpha} \tag{127}$$

for velocity proportional stoppers.

Robertson (Ro 69) has shown that for the particular case of ^{39}K stopping in K I, the correction to $F(\tau)$ due to strong nuclear stopping is about 25%. Since the masses of both the recoil and stopping nuclei are the same one would expect nuclear stopping to be large for this case and, hence, the 25% error in (127) for other cases to be an upper limit.

CHAPTER 2

DETECTORS

2.1 Neutron Detector

The neutron detector consists of a liquid organic scintillator (NE 218) in a chamber viewed by an RCA 8575 photomultiplier providing a fast 50 ohm impedance dynode output and a slow linear 100 ohm anode output. Inputs to this unit are the high voltage connection to the photomultiplier section and the pre-amplifier and discriminator inputs. The fast signal, so called because it is taken from a dynode in the photomultiplier amplification chain and, thus, is spared R-C shaping involving long time constants, is used for timing purposes after it is passed through a walk-free timing discriminator (rise time of this timing signal T_r < 2 n.s. and the pulse width $T_W \approx$ 10 n.s.). The anode signal is taken to a preamplifier and integrated so that the output rise time is approximately 50 n.s. and is suitable for processing by an R-C shaping amplifier.

The scintillator responds to both gamma rays and neutrons so that for n-γ coincidence work, methods must be found to identify the gamma rays and also, if possible, to separate the gamma ray linear signals from

the neutron signals (pulse shape discrimination). The pulse shape discrimination determines what radiation dependent effects combine to produce the scintillations in order to correlate the observed events with the type of radiation incident on the detector.

Organic scintillators are composed of hydrogen (proton) rich molecules (the specific case here, NE 218, has a proton-carbon ratio of 1.4). Scintillations are produced when either a proton or an electron produces "excited" molecules along its flight path through the liquid. This "excitation" is of two types (Br 59) - electronic excitation and ionization.

Electronically excited molecules, M*, decay by two processes:

1. $M^* \rightarrow M + \text{photon}$
2. $M^* \rightarrow M + \text{heat (vibrational energy)}$ (A)

Ionization, however, involves an additional step:

$$M^+ + e^- \rightarrow M^* \qquad \text{(B)}$$

with M* decaying by either process 1 or 2 of (A).

Process (B) involves the recombination of the ion with an electron and thus is governed by the relatively slow diffusion of electrons (recombination time $\gtrsim 10^{-7}$ secs.), whereas, process (A) takes of the order of 10^{-9} secs. to complete. The light intensity of both

processes(A) and (B) are exponential decays in time.

It has been shown (Ta 51) that the light output or pulse height in an organic scintillator is not proportional to the particle energy and, in fact, is less for a proton than for an electron of the same energy. The light output is actually a function of the density of M^+ and M^* along the trajectory of the particle and it is here that different modes of quenching (other than 1 of (A)), through interactions (of type 2, for example) between excited ions of molecules, can occur, thus lowering the light output since type 1 is the only photon producer. Clearly, a heavier particle is going to leave a higher density of excited molecules in its wake than a lighter particle of the same energy and the light output from protons is less than that from electrons since the former case the greater density of excited molecules permits quenching by processes other than type 1.

The scintillations may now be divided into two types: a fast component, F, which is attributable to process 1 of (A), and a slow component, S, from process (B). The decay time of F is usually several nanoseconds while for S it is about 100 n.s. Further, as has been stated before, one expects more photons, f_e, from the

electrons than the number, f_p, from the protons ($f_p < f_e$).

The production of the slow component, S, has two effects: one is that it is, by the nature of the recombination process, slow, and the other is because it is so slow, the M* formed through process (B) arrive in a situation where the density of initially excited molecules (usually formed through (A) and hence have fast decay times) is much lower than it was at the beginning of excitation so that the probability of type 1 occurring is greatly enhanced over process 2. Therefore, by the previous argument, more "slow" photons S_p are usually expected from protons than the number S_e from electrons. Although it is still possible for $S_p < S_e$ the ratio $S_p/S_e > f_p/f_e$ so that $S_p/(f_p + S_p)$, the proportion of S from proton scintillations is greater than $S_e/(f_e + S_e)$ from electron scintillations.

Now, one need only recall that gamma rays produce recoil electrons (photoelectrons, Compton electrons, or pair-produced electrons and positrons) and neutrons produce recoil protons, to conclude that gamma-originated scintillations will have less slow component than neutron-originated scintillations (figure 4).

In delay line shaping the input signal is divided into two branches: in one branch the signal current is unaffected but in the other the inserted delay line

Figure 4. All vertical scales are pulse amplitudes and all horizontal scales are time.

(a) Solid line represents a neutron scintillation with an exponential decay having fast (F) and slow (s) components and the dotted continuation completes the gamma ray produced scintillation (almost entirely fast component).

(b) Preamplification of (a).

(c), (d), and (e), (f) show the process of single delay line shaping applied twice resulting in separate crossover points (t_F, t_s) for the gamma ray originated pulse and the neutron pulse.

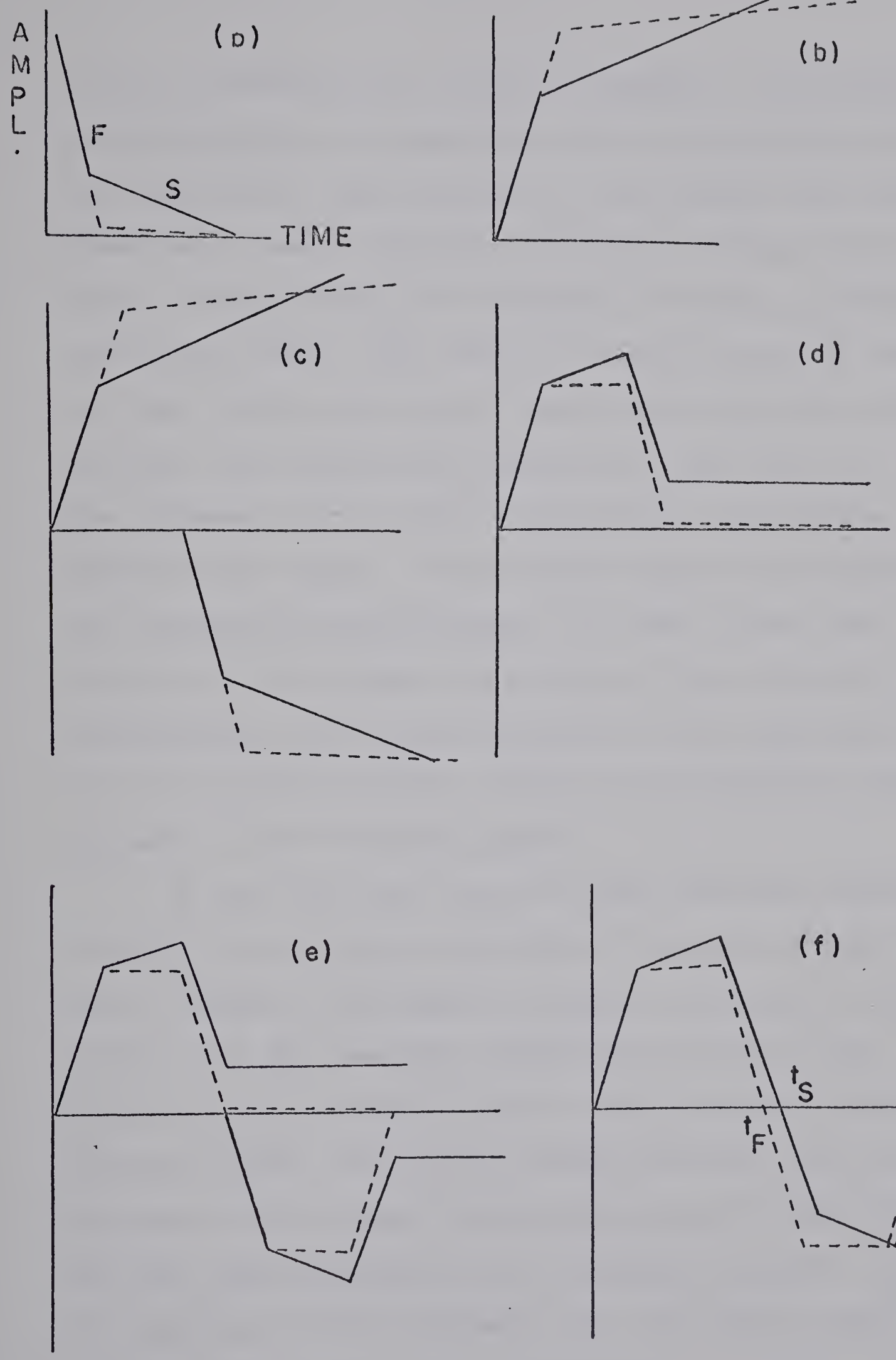

FIGURE 4

inverts and delays the signal. Resistors are placed in both branches to compensate for the attenuation of the delay line. The currents in the branches are then summed at a common junction, producing a shaped output signal. Double delay line shaping, of course, performs the process twice. The effect is shown (figure 4) for two input pulses (one with a large slow component and one with very little slow component). The effect of the slow component is to cause an incline to the plateau region of the signal. After double delay line shaping this results in a displacement, in time, of the zero crossover of the signal and by using a zero crossing discriminator, fast timing signals will be generated at the two crossover points. Neutron identification then proceeds in the following manner.

A zero time mark may be derived from the neutron detector discriminator output which takes its signal from a dynode at the onset of charge collection at the anode (it is the same for either the neutron or the gamma ray) and is used to start a time-to-pulse height converter (TAC). The timing signals derived from the crossover of the shaped linear pulse stop the TAC and the time spectrum obtained will contain two peaks - one for neutrons and one for gamma rays, and may be used as a neutron identifier for the detector.

The scintillator-photomultiplier is used most advantageously in fast timing applications because of its excellent timing resolution. This resolution, however, is governed by four main factors (Re 61):

a) variation of the time of interaction of the radiation with the scintillator and the amount of energy deposited therein (detected thickness contributes to this);

b) the finite decay times of the light emitting states in the scintillator and variation of the times of photon arrival at the photo-multiplier cathode due to optical reflections and absorption within the scintillator chamber which are determined by the geometry of the chamber and by the optical coupling of the scintillator to the photomultiplier;

c) the variation of the transit time of the photo-electrons in the photomultiplier due to the different path lengths and the variation of the critical energy and angle of the secondary electrons; and

d) the jitter and uncertainty of the times of triggering of associated electronics.

2.2 Lithium Drifted Germanium Detector

A simple semiconductor detector consists of a junction between n-type material, where virtually all the charge carriers are electrons, and p-type material, where they are all holes (this is basically a diode). Where the two are joined some of the holes from the p-layer diffuse into the n-layer, and some of the electrons from the n-layer diffuse into the p-layer, the process constituting an electric current flowing from the p to the n region and clearly cannot continue indefinitely without power. The current is inhibited by the built-in voltage arising from ionized impurities in each region. If this diode is reverse-biased the holes will be forced into the p-region and electrons into the n-region creating a depletion layer which is charge free. One should note that one way of creating intrinsic material from substances such as germanium or silicon having p-type impurities is to drift the material with an n-type material such as lithium.

To find the depletion layer thickness one has to solve Poisson's equation. For p-type material this becomes (in one dimension) (De 63)

$$\frac{d^2V}{dx^2} = \frac{4\pi e}{\chi} (N_A + n - p) \qquad (1)$$

where V(x) is the potential difference across the p-region, χ is the dielectric constant of the crystal, N_A is the acceptor impurity concentration, n and p are the local electron and hole densities.

Since in actual fact n and p are not constants, solution of (1) will present a rather tedious problem, so it will be assumed that n and p are small compared to N_a throughout the depletion region (a poor approximation). Integrating (1) twice one finds that

$$V(x) = \frac{4\pi\ e\ N_A}{\chi}\ (x^2 - 2x\ x_p) + V_o \qquad (2)$$

where x_p is the termination of the depletion region where $N_A + n - p = 0$ and $V_o \equiv V(0)$ is the potential at $x = 0$, the junction interface. Thus at $x = x_p$, $V - V_o = V_p$, the potential difference across the p-region. Therefore,

$$x_p^2 = \frac{V_p\ \chi}{2\pi\ N_A\ e} \qquad (3)$$

is the thickness of the p-region and,

$$x_n^2 = \frac{V_n\ \chi}{2\pi\ N_D\ e} \qquad (4)$$

is the thickness of the n-region, where N_D is the donor impurity concentration and V_n is the potential across

the n-layer. In actual cases, the ionized impurity concentration is very different on the two sides of the junction and the depletion thickness resides almost entirely within one type of material. For n-type material the width will be given by

$$x^2 \approx \frac{\chi}{2\pi e} \frac{V}{N_D} \quad . \tag{5}$$

The resistivity of the n-type material will be given by

$$\rho = \frac{1}{N_D e \mu_n} \tag{6}$$

where μ_n is the electron mobility in the crystal and,

$$\mu_n = \frac{v_e}{E} \quad , \tag{7}$$

E being the applied electric field and v_e the velocity of the electron, and is given by

$$E = J \rho \quad , \tag{8}$$

J, of course, is the current density and may be expressed in terms of N_D and v_e:

$$J = N_D v_e e \quad . \tag{9}$$

Equations (7), (8), and (9) combine to give (6), and (6) with (5) gives

$$x \approx \sqrt{\frac{\chi \mu_n \rho V}{2\pi}} \quad . \qquad (10)$$

This brief description, of course, is for a planar detector, whereas the actual detector used was co-axial, the situation being considerably more complicated. The principle, however, is basically the same and one usually has a p-type core with lithium drifted radially inwards to form an n-type cylindrical layer.

The depletion region behaves in an analogous manner to an ionization chamber since a charged particle incident upon the region loses energy creating hole-electron pairs which are swept out by the applied field, the charge being collected as a function of time. On the average, it takes about 3.5 eV of energy lost by the incident particle to create one hole-electron pair in silicon and since this is constant, the energy of the particle will be proportional to the total charge it produces. Photons are detected in the crystal by the transfer of their energy to charged particles in the detector. This interaction is governed by three processes by which photons interact with matter: the photoelectric effect, where all the energy of the photon is transferred to a photoelectron; the Compton effect,

Figure 5. The basic time walk problem of a simple discriminator is illustrated for two pulses of amplitudes V_1 and V_2.

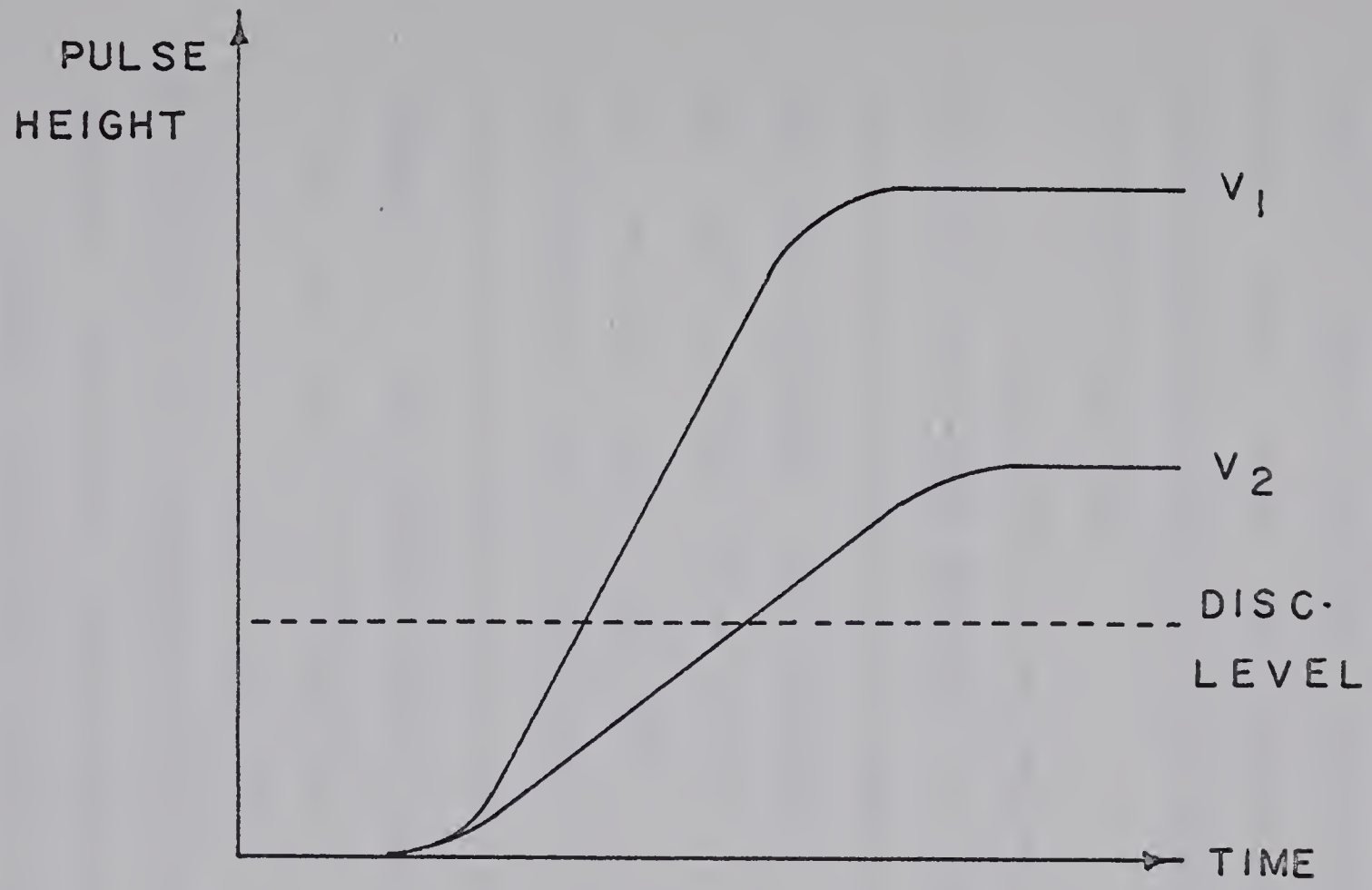

FIGURE 5

where part of the photon energy is transferred to an electron and the photon of reduced energy is scattered; pair production, where the photon energy is used to create an electron-positron pair having some kinetic energy. Thus, the Ge (Li) detector may be used as an energy sensitive device for the detection of photons and charged particles.

It is possible to use pulses from Ge (Li) detectors for timing purposes, as well, providing the signals are processed in the proper manner to eliminate time walk problems. This problem is typical of leading-edge timing systems where a timing signal is produced when the input signal amplitude rises above a pre-set discriminator level. Variations in amplitude lead to shifting of the timing point along the time axis (figure 5). The problem can be very drastically reduced if one could cause the discriminator level to move up and down with the pulse amplitude so that the time mark is generated at a constant fraction of pulse height (constant fraction of pulse height trigger or C.F.P.H.T.).

Another problem that spoils the time resolution of the Ge (Li) detector is the variation of pulse shapes due to the fact that charged particle interactions occur at different locations within the depletion region

Figure 6. A planar detector of width W separating the n^+ and p layers (depletion region) is shown biased with V volts. x is the location of the ionization and the motion of the resulting holes (h^+) and electron (e^-) is indicated.

The pulse shapes for ionizations occurring at positions A and B in the depletion layer are depicted for the case $\mu_e = \mu_h$.

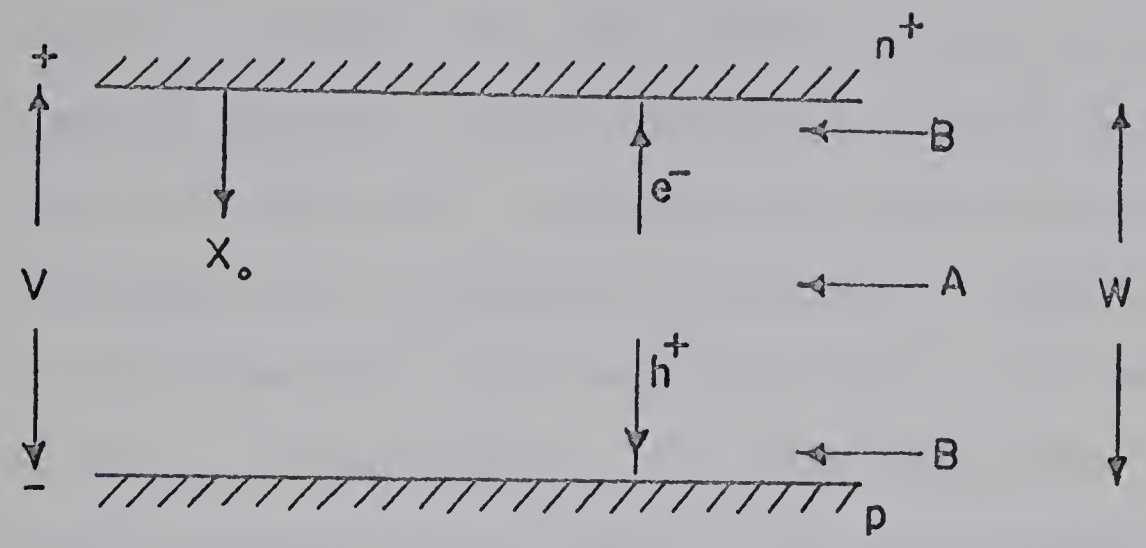

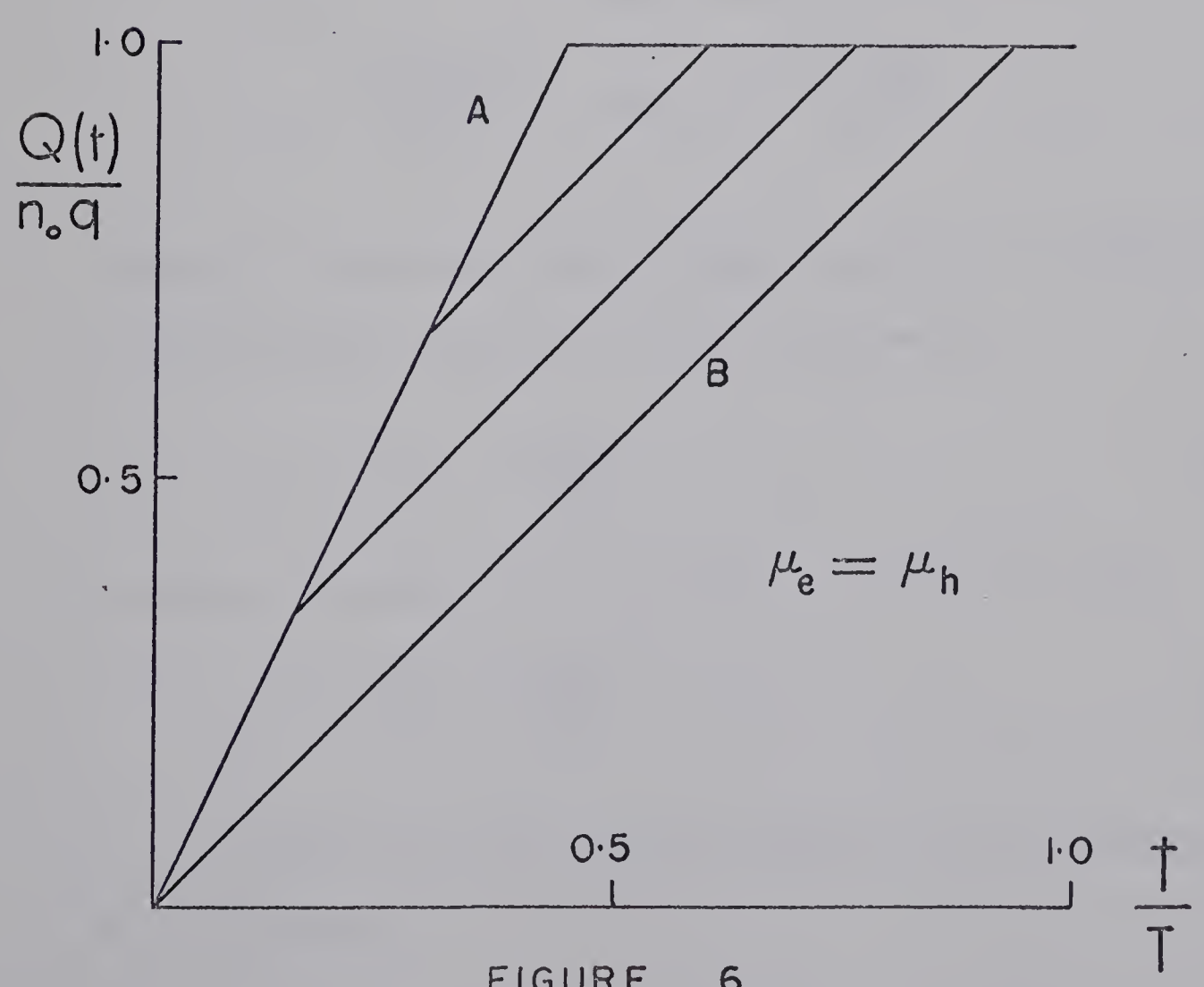

FIGURE 6

(Sa 68). To see this more clearly (figure 6a) consider a planar detector with a depletion region, i, of total width, W, and with a charged particle interaction occurring at a distance x_o from the n^+ layer producing n_o hole-electron pairs each of charge q and mobility μ_h and μ_e respectively. t is the time after ionization and the quantities t_e and t_h will be defined as follows,

$$t_e = t \qquad \text{for } t \leq \frac{W\, x_o}{\mu_e\, V}$$

$$t_e = \frac{W\, x_o}{\mu_e\, V} \qquad \text{for } t > \frac{W\, x_o}{\mu_e\, V}$$

$$t_h = t \qquad \text{for } t \leq \frac{W(W-x_o)}{\mu_h\, V}$$

$$t_h = \frac{W(W-x_o)}{\mu_h\, V} \qquad \text{for } t > \frac{W(W-x_o)}{\mu_h\, V} \quad ,$$

since the velocity for a charge carrier of mobility μ in an electric field $E = V/W$ is given by

$$v = \mu E = \frac{\mu\, V}{W} \quad , \tag{11}$$

so that the time, t, to travel a distance x is

$$t = \frac{x}{v} = \frac{W\, x}{\mu\, V} \quad . \tag{12}$$

Let T be the time to travel over the entire width W. Therefore,

$$T_e = \frac{W^2}{\mu_e V} \tag{13}$$

for electrons and,

$$T_h = \frac{W^2}{\mu_h V} \tag{14}$$

for holes. Hence the ratio of the charge collected after time, t, to the total charge produced at ionization is given by

$$\frac{Q(t)}{n_o q} = \frac{t_e}{T_e} + \frac{t_h}{T_h} \tag{15}$$

a plot of which is seen in figure 6b where some typical pulse shapes are illustrated. The pulse shapes are characterised by an initial fast rise until one type of carrier has been swept out of the depletion region, followed by a rise at half of the former rate of charge collection until the other type of carrier reaches its appropriate layer. Of course, the possibility of Compton scattering and multiple interactions has not been considered, the effect being to complicate the shapes of the pulses. There will still be a fast and a slow component to the pulses, however.

For the case of a co-axial detector having an n^+ layer and a p-type core the situation is made quite complicated because of the 1/r dependence of the electric

field. Electrons are accelerated outwards by a decreasing field and holes inwards by an increasing field. The result is that ionizations occurring close to the n^+ layer tend to produce pulses with slow rise times whereas events midway between the n^+ and p layers, in a considerably wide band, produce pulses with relatively fast rise times. Events close to the core produce pulses with initially fast rise times to about $Q(t)/n_o q \approx 0.5$ with slow components taking over until the total charge is collected.

The effect of this pulse shape distribution is to cause non-amplitude related timing uncertainties which cannot be entirely compensated for by the C.F.P.H.T. Placing an annulus of lead over the outer regions of the detector will help suppress slow rising pulses by partial elimination of ionizations in that location, but the effect will not be great and the disadvantage will be a drastic reduction in the Ge (Li) efficiency since from purely geometrical considerations, one can see that a large fraction of the total number of events originate in this region. Another method to improve the time resolution might be to use a rise time spectrometer and a computer to select pulses according to their rise times so that separate time pickoffs can be used for groups of pulses with similar rise times.

CHAPTER 3

EXPERIMENTAL ASPECTS OF THE ^{53}Mn LIFETIME MEASUREMENTS

3.1 Introduction

This experiment is concerned with the measurement of the lifetimes of the bound levels of ^{53}Mn through the ^{53}Cr (p, n γ) ^{53}Mn reaction using the DSAM method. Although the DSAM method may be employed without the neutron-gamma ray coincidence, the inclusion of this condition greatly simplifies the analysis of the data. This results from the reaction kinematics which show that if only a narrow cone of neutrons is detected in, say, the backward direction (from the incident beam direction) then the de-excitation gamma rays in coincidence with these neutrons will be from recoil nuclei travelling in a much narrower cone in the forward direction (for this experiment with 5.5 MeV protons the recoil nuclei will subtend a half-angle of less than 4° if the neutron detector subtends a half-angle of 20°). Thus, the effect on the gamma ray Doppler shifts due to the initial angular dispersion of the recoil nuclei is much more easily calculated for the case of the narrow cone than for an isotropic angular

Figure 7. The electronics set up is shown.

(1) R-C amplifier (input from the Ge (Li)) (Ortec Model 450).

(2) Single channel analyzer (Ortec Model 406).

(3) Timing filter amplifier (accepts timing signals from the Ge (Li)) (Ortec Model 454).

(4) Constant fraction timing discriminator (C.F.P.H.T.) (Ortec Model 453).

(5) Gate and delay generator (Ortec Model 416).

(6) Time to amplitude converter (Ortec Model 437).

(7) Double delay line amplifier (Ortec Model 410).

(8) Fast zero crossing discriminator.

(9) Time pickoff control (Ortec Model 403A).

(10) Universal coincidence units (Ortec Model 418).

(11) Timing single channel analyzer (Canberra Model 1436).

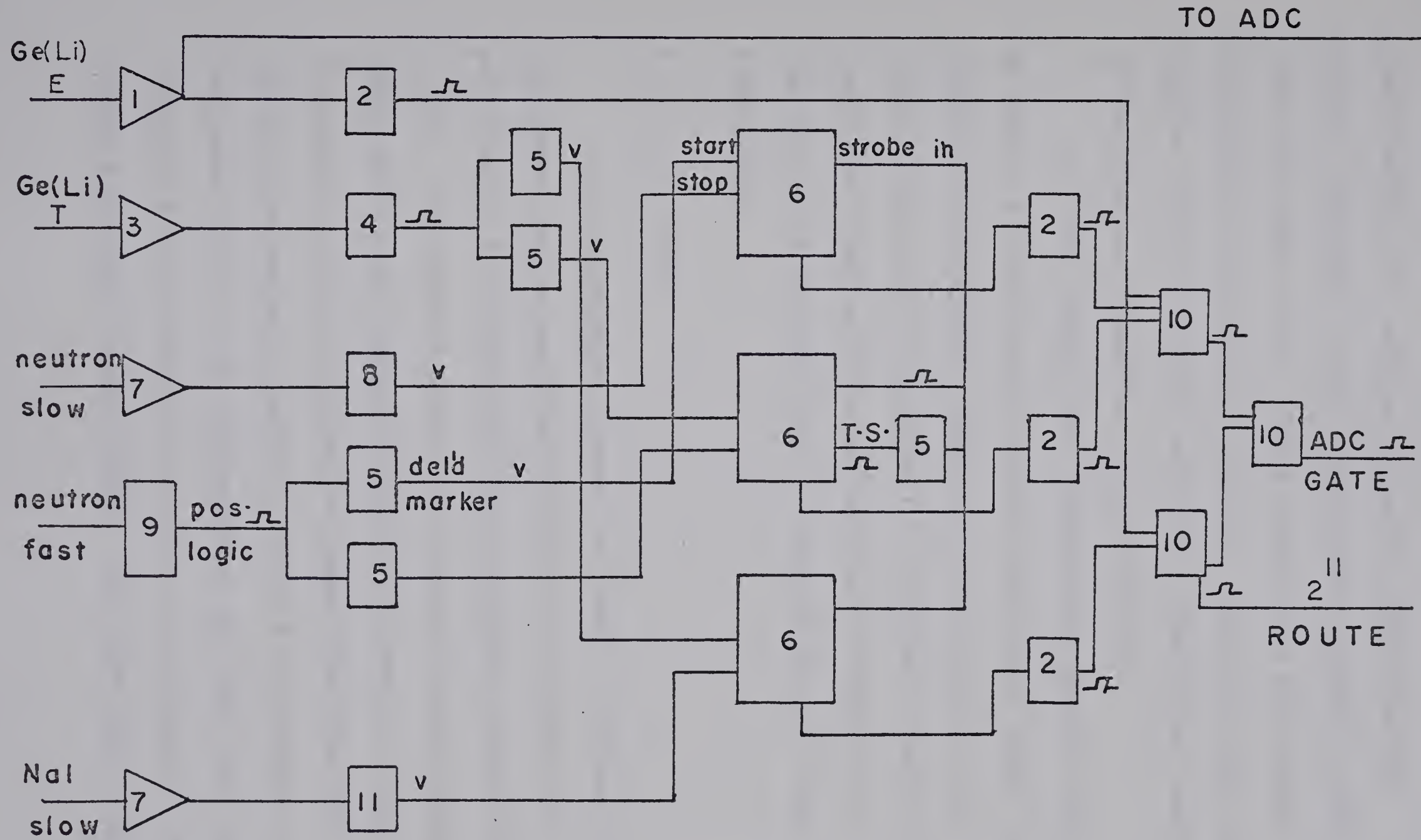
TO ADC
Ge(Li)
E
1
2
Ge(Li)
T
3
4
5
V
5
V
start
stop
6
strobe in
2
10
neutron
slow
7
8
V
6
T·S·
5
2
10
ADC
GATE
neutron
fast
9
pos.
logic
5
dela
marker
V
5
6
2
10
2
11
ROUTE
Nal
slow
7
11
V

FIGURE 7

distribution (no neutron-gamma ray coincidence). Another advantage of the coincidence method is that since the only recoil nuclei considered are those confined to the forward direction they will have the highest initial velocity and will, therefore, result in the greatest possible Doppler shifts.

In this chapter the electronics system required to obtain a calibrated, neutron-coincident gamma ray spectrum (using pulse shape discrimination in the neutron detector as discussed in Chapter 2) will be described along with the mechanical arrangement of the detectors and the type of targets used in the experiment.

3.2 Electronics

The electronics system is shown in figure 7. The gamma ray pulses from the Ge (Li) detector are put into an R-C amplifier with a shaping constant of 2 μ.s., the outputs going to a single channel analyzer (SCA) and to the analog-to-digital converter (ADC). A window is set on the desired gamma spectrum with the SCA the output of which goes to a coincidence unit. The gamma pulses from the detector are also put into a timing and filter amplifier (TFA) to be properly R-C shaped for input to the CFPHT. The slow logic signal

thus derived, is then passed on to two gate and delay units, the delayed marker of one going to the gamma-gamma TAC, the other going to the start input of the n-γ TAC the stop coming from the fast neutron detector output. The output of this TAC gives the n-γ time spectrum. The extra gate and delay in the fast neutron side is to provide maximum flexibility in the adjustment of the delays. The gamma ray pulses from the sodium iodide (Na I) detector (which is shielded with lead so that it views only a ^{60}Co source whereas the Ge (Li) detector views both the ^{53}Cr target and the source) are double-delay-line shaped and then a timing SCA (TSCA) is used to put a window on the two source lines. The fast output of the TSCA goes to stop the γ-γ TAC, the output of which goes to the same coincidence unit as before (coincidence requirement of 2). Hence, a gamma ray coming from the source (within the ^{60}Co window) and a gamma from the target (within the spectrum window) will cause the coincidence unit to deliver an output going to the final coincidence unit and to the 2" route of the kicksorter, meaning that the gamma spectrum with the source spectrum included will be put into the next 2048 channels from the primary n-γ coincidence spectrum. The neutron linear signal is passed through a fast zero crossing discriminator (FZCD) which delivers

early pulses for gamma ray pulses and late pulses for neutron signals into the stop input of the neutron identifier TAC which is started by the neutron detector discriminator pulse occurring for both neutrons and gamma rays. The output of the TAC will contain two peaks - one for neutrons and the other for gamma rays, counted in the detector. Windows are placed on the neutron identifier peak and on the neutron peaks of the n-γ time spectrum using SCA's, the pulses of which are placed in coincidence with the gamma spectrum window (3-fold coincidence requirement) in a coincidence unit which provides a true n-γ signal. This signal and the γ-γ signal are both fed into a common gate having a single coincidence requirement so that either signal opens the ADC gate. The gamma rays which are in coincidence with the neutrons appear in the first 2048 channels of the kicksorter. A feature of the n-γ TAC that provides a true start has been used. The true start signal is delayed and then used to strobe all three TAC's at the same time, if and only if a stop signal at the n-γ TAC has been preceded by a legitimate start signal. This feature is advantageous where high count rates are prevalent such as the neutron detector since it detects both neutrons and gamma rays. Recording the independent γ-γ spectrum with its unchanging

^{60}Co peaks allows one to monitor any gain shifts that may occur as a result of electronic instabilities in the system.

3.3 Experimental Arrangement

The neutron detector was placed at approximately 180^{o} and 15 cm. back from the target (a hole in the center of the detector permitted this) and the entire face of the detector opposite the target was shielded with lead to reduce the gamma ray flux into the scintillator. The fast and linear outputs were connected, with 50 Ω and 100 Ω coaxial cable, respectively, to the electronics in the control room. The detector was then biased at -2250 volts and the discriminator was set just above the self-triggering level. The Ge (Li) detector was placed on a rotatable platform, the center of rotation lying directly below the target. Lead was placed over the face of the detector to reduce the excessively high count rate produced by low energy gamma rays, and the detector was biased after all the preamplifier connections had been made.

About 30 cm. directly above the Ge (Li) detector was placed the Na I detector, the ^{60}Co source being situated midway between the two. The Na I detector was shielded with lead to prevent viewing of the target-originated gamma rays. The system permits spectra to be

taken at 0^{o} and $\gtrsim$ 120^{o} to obtain shifts of the order of $1.5\overline{\Delta E}_{\gamma}$ (see figure 8 and figure 9).

3.4 Targets

Two types of targets were made. One type involved a simple evaporation of a small amount ($\lesssim 0.5$ mg/cm^2) of Cr enriched to 96% ^{53}Cr onto a support backing of tantalum (0.005" thick). The range of the recoil ions in ^{53}Cr (see Chapter 4) was determined to be approximately 0.01 mg/cm^2 for an initial recoil energy of about 300 KeV. Also it was calculated that the beam would lose about 5 KeV of its original energy in passing through the target, giving very little uncertainty in the recoil ion starting velocity. However, in order to be absolutely sure all the ions are stopped in the target material a target thickness of several hundred times the recoil range is desirable.

Thus a second type of target was made by first evaporating a layer of natural chromium to a thickness of approximately 6 mg/cm^2 (natural chromium contains about 6.5% ^{53}Cr) followed by about 0.5 mg/cm^2 of ^{53}Cr. The change in slowing down time caused by the differing mass numbers will effectively be far less than 2% since the great majority of the ions will be stopped in the ^{53}Cr layer. The beam dispersion, however,

will be approximately 50 KeV resulting in a small uncertainty in the starting velocity, and may necessitate interpolation between $F(\tau)$ curves resulting from different assumed starting velocities.

Figure 8. The side of the basic mechanical arrangement of the experiment is shown:

(1) portion of the Na I detector shielded with lead from the target gamma rays;

(2) ^{60}Co source location;

(3) portion of the Ge (Li) detector;

(4) beam line;

(5) neutron detector shielded on both faces with lead (hatched line);

(6) target inside the target pot assembly (joined to the beam line behind the neutron detector).

The entire assembly of (1), (2), and (3) rotates together about the target (dotted line indicates the vertical axis of rotation).

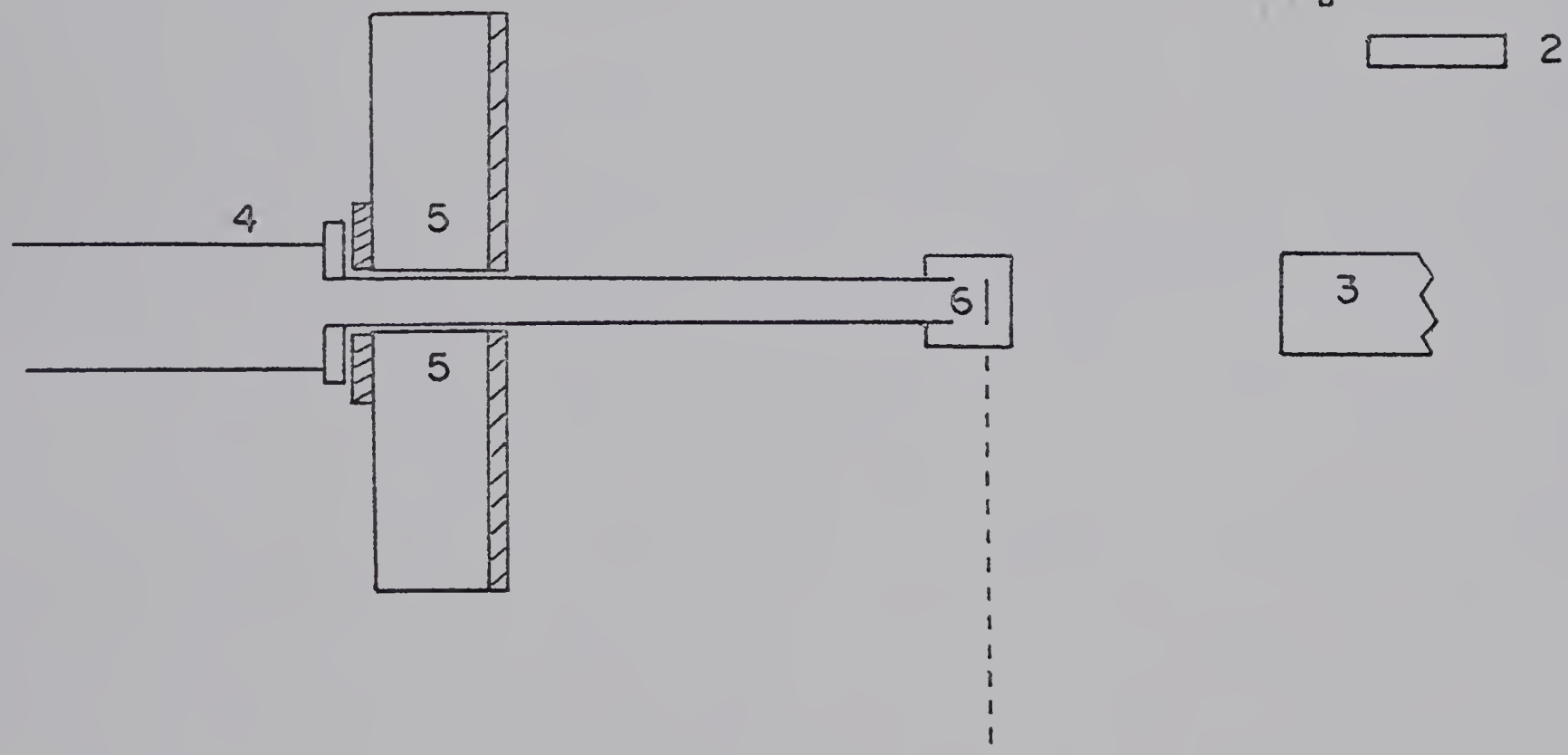

FIGURE 8

Figure 9. The top view of the experimental assembly is shown.

(1) Ge(Li) and Na I detectors;

(2) target and target pot;

(3) neutron detector with photo-multiplier,

(4) attached;

(5) beam line.

An outline of the correlation table is illustrated.

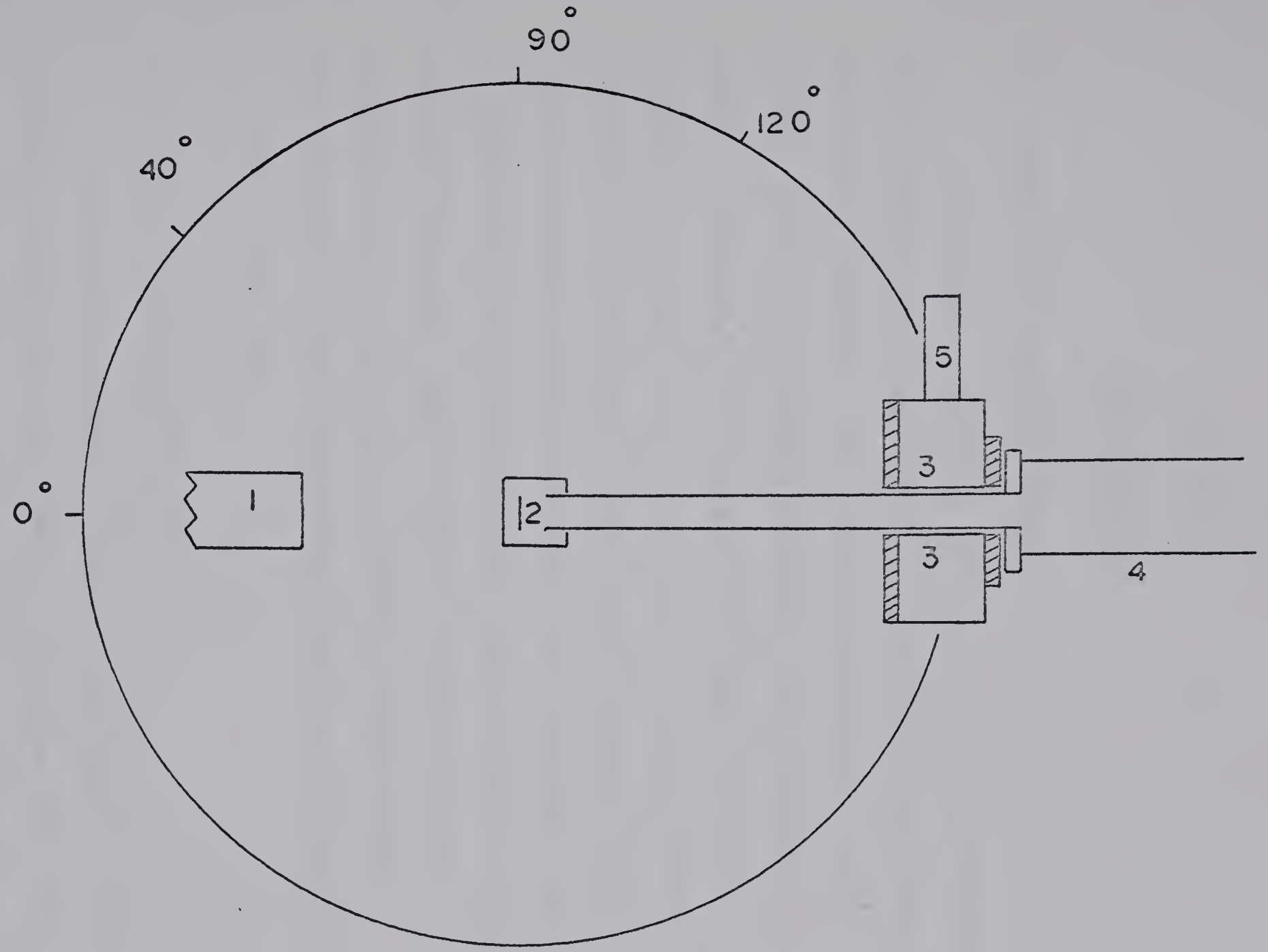

FIGURE 9

CHAPTER 4

DATA ANALYSIS

4.1 Range and Stopping Powers

A program (DEDX) was written in APL to determine the stopping power and range according to the Lindhard or Firsov formulae. The range calculations for the recoil ions in the target material are necessary in order to determine the target thickness required to stop all the ions in the substance. A target that is too thin will lead to some vacuum recoils which make the DSAM results incorrect. On the other hand, a target that is too thick will cause excessive beam energy dispersion which leads to uncertainty in determining the starting velocity of the recoils. The accuracy of the information from these formulae is better than 20%.

4.2 Reaction Kinematics and $F(\tau)$

A Fortran program (DSAM 1A) calculating relativistic kinematics was used to determine the initial velocity of the recoil ions. The neutron detector subtends a half-angle of about 20^{o} so that only neutrons falling within this were considered which, of course,

fixed the direction and energy of the recoil ions for a particular excited gamma ray level. Since the neutron angles considered in the kinematics were 180^{o}, 170^{o}, and 160^{o}, an average of the three corresponding recoil starting velocities was taken. The variation among these velocities for a particular level were typically less than 3%, this fact being the empirical justification for the simple averaging process. These were weighted with the $E_{\gamma o}$ cos θ term to determine the full kinematic shift for θ equal to 0^{o} and 120^{o}, and 0^{o} and 90^{o} ($\Delta E_{\gamma o}$).

$E_{\gamma o}$, of course, is the unshifted gamma ray energy and can be determined accurately by measurement of the gamma ray at a forward and a backward angle. At the forward angle, θ_f, the energy, $E_{\gamma f}$, will be Doppler shifted up from $E_{\gamma o}$. Thus one has

$$E_{\gamma f} = E_{\gamma o} (1 + \Delta \cos \theta_f) \qquad (1)$$

where Δ is the Doppler shift attenuation factor. Similarly for the backward measurement one has

$$E_{\gamma b} = E_{\gamma o} (1 - \Delta \cos \theta_b) . \qquad (2)$$

Hence

$$E_{\gamma f} + E_{\gamma b} = 2 E_{\gamma o} + E_{\gamma o} \Delta (\cos \theta_f - \cos \theta_b) \qquad (3)$$

and

$$E_{\gamma f} - E_{\gamma b} = E_{\gamma o}\, \Delta\, (\cos\theta_f + \cos\theta_b) \quad . \qquad (4)$$

Therefore, using (3) and (4), the unshifted gamma ray energy will be given by (Ro 69),

$$E_{\gamma o} = \frac{E_{\gamma f} + E_{\gamma b}}{2} - \frac{E_{\gamma f} - E_{\gamma b}}{2} \left(\frac{\cos\theta_f - \cos\theta_b}{\cos\theta_f + \cos\theta_b}\right) \quad . \qquad (5)$$

The $F(\tau)$ values were calculated using an ALGOL program written by Robertson (Ro 69) using various approximations (see Chapter 1, nuclear stopping) and truncations of integrals. These values agree with Blaugrunds calculations to within 10% over most of the range of $F(\tau)$. The values were plotted on semi-logarithmic graph paper as a function of τ (figure 15) and are used to determine the lifetimes of the states studied. The accuracy of the calculated $F(\tau)$ values should be within 15% to 20%.

4.3 Centroid Analysis

An APL program (BACK) was written to manipulate single gamma ray peaks (background included) and perform background subtraction (two independent linear background fits may be chosen, one for the high energy

side of the peak and one for the low energy side, these being used to help determine manually chosen points through which a linear fit is made to form the background under the peak), peak plotting (with errors), peak summation with errors, and centroid calculation with its inherent error. The contribution to the centroid error by uncertainties in determining the proper background was estimated by variation of the background within reasonable limits and examination of the resultant change in the centroid. The total error, then, is simply the sum in quadrature of these errors.

CHAPTER 5

THE ^{53}Mn LIFETIME EXPERIMENT

5.1 5.2 MeV protons from the University of Alberta van de Graaf accelerator were used to bombard the Cr target and initiate the ^{53}Cr (p, nγ) ^{53}Mn reaction. In order to obtain a reasonable coincidence rate and still retain good energy resolution in the Ge (Li) a count rate in the Ge (Li) of approximately 8×10^3 sec.$^{-1}$ was maintained throughout the experiment requiring a D.C. beam intensity of 70 nA. Coincident gamma rays were observed from about 600 KeV in energy to 3100 KeV. A one hour singles run was taken at an angle of 90^{o} to determine the zero-shifted gamma rays. The Doppler shifted gamma rays were obtained with a five hour coincidence run at zero degrees. Using an auxiliary kicksorter, the SCA windows set on the TAC spectra were periodically checked for evidence of drifting (see figure 10 and figure 11).

5.2 Results

The following gamma rays were observed in the coincidence and the singles spectra:

Figure 10. This is the neutron time-of-flight spectrum from the TAC using coincident gamma rays as the zero time mark (large peak). To the left of this peak are a large number of very small peaks forming the neutron groups. The time resolution is not good enough to resolve a particular group responsible for populating a level in the residual nucleus.

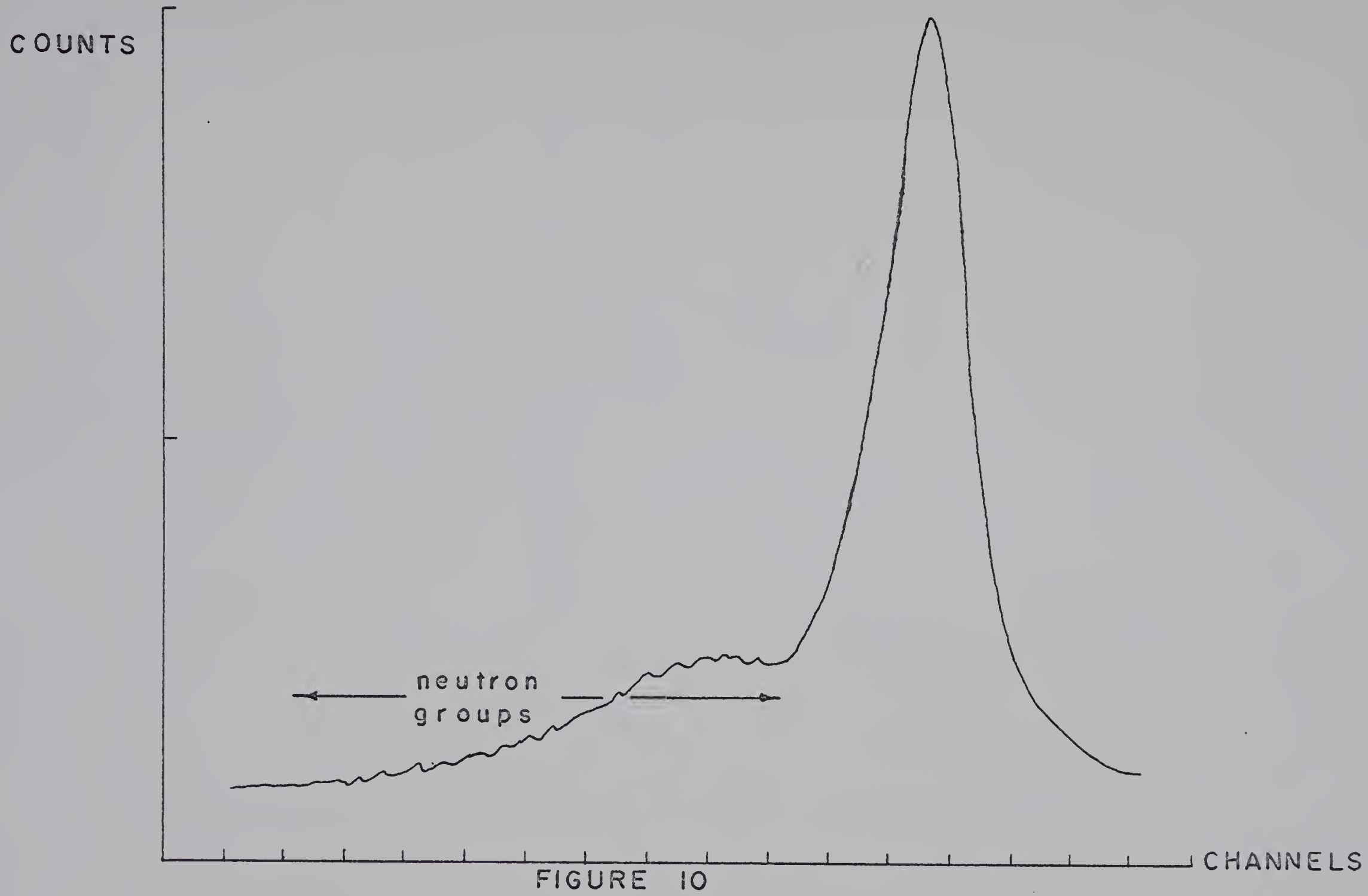

FIGURE 10

Figure 11. The neutron identifier time spectrum from the TAC is shown and results from the different amounts of "slow" component in gamma ray and neutron scintillations in the organic liquid detector. The neutron counts have been raised by a factor of 10 for illustrative purposes.

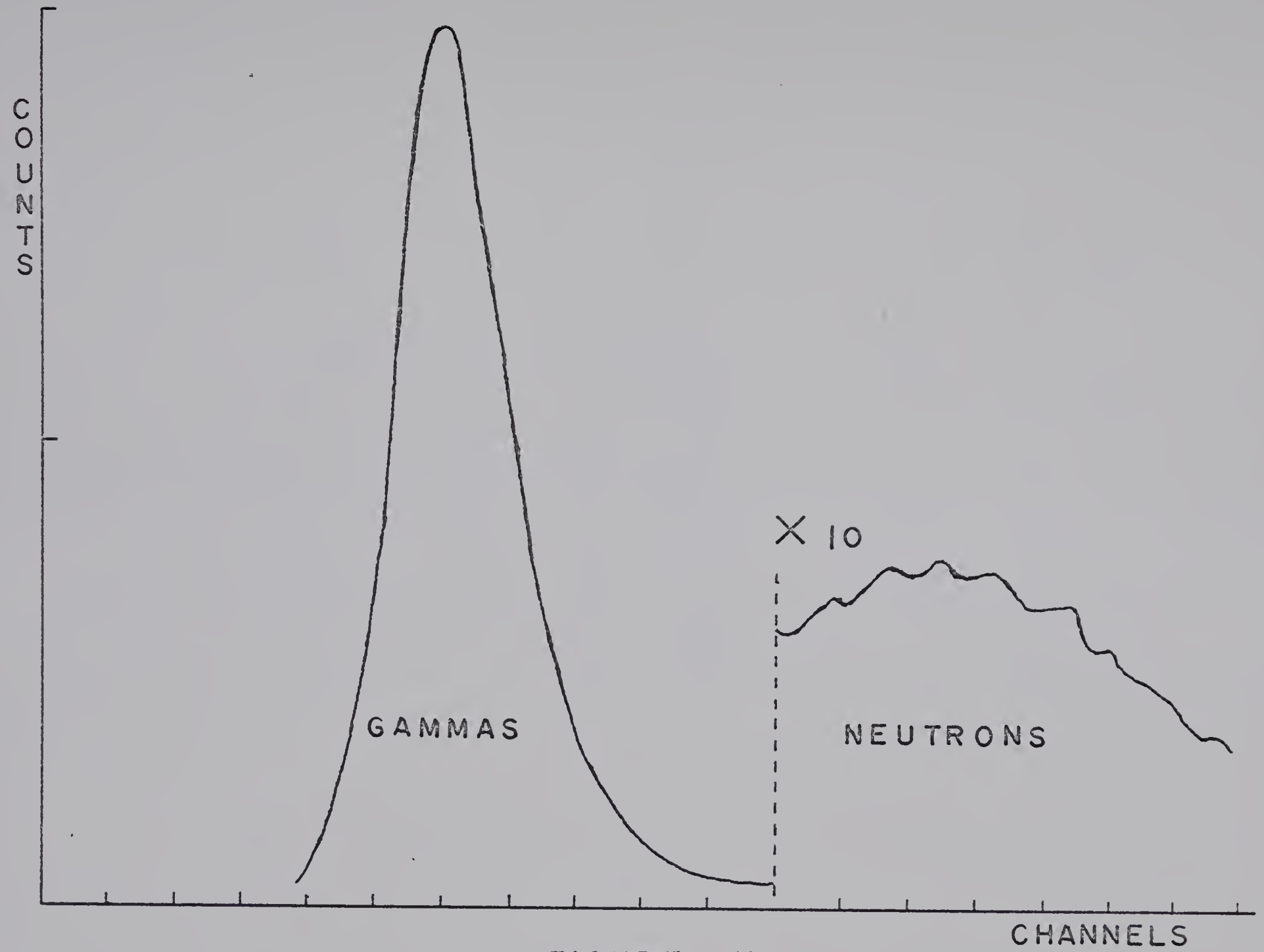

FIGURE 11

Figure 12. The portion of the decay scheme of ^{53}Mn considered for this experiment is shown here.

^{53}Mn

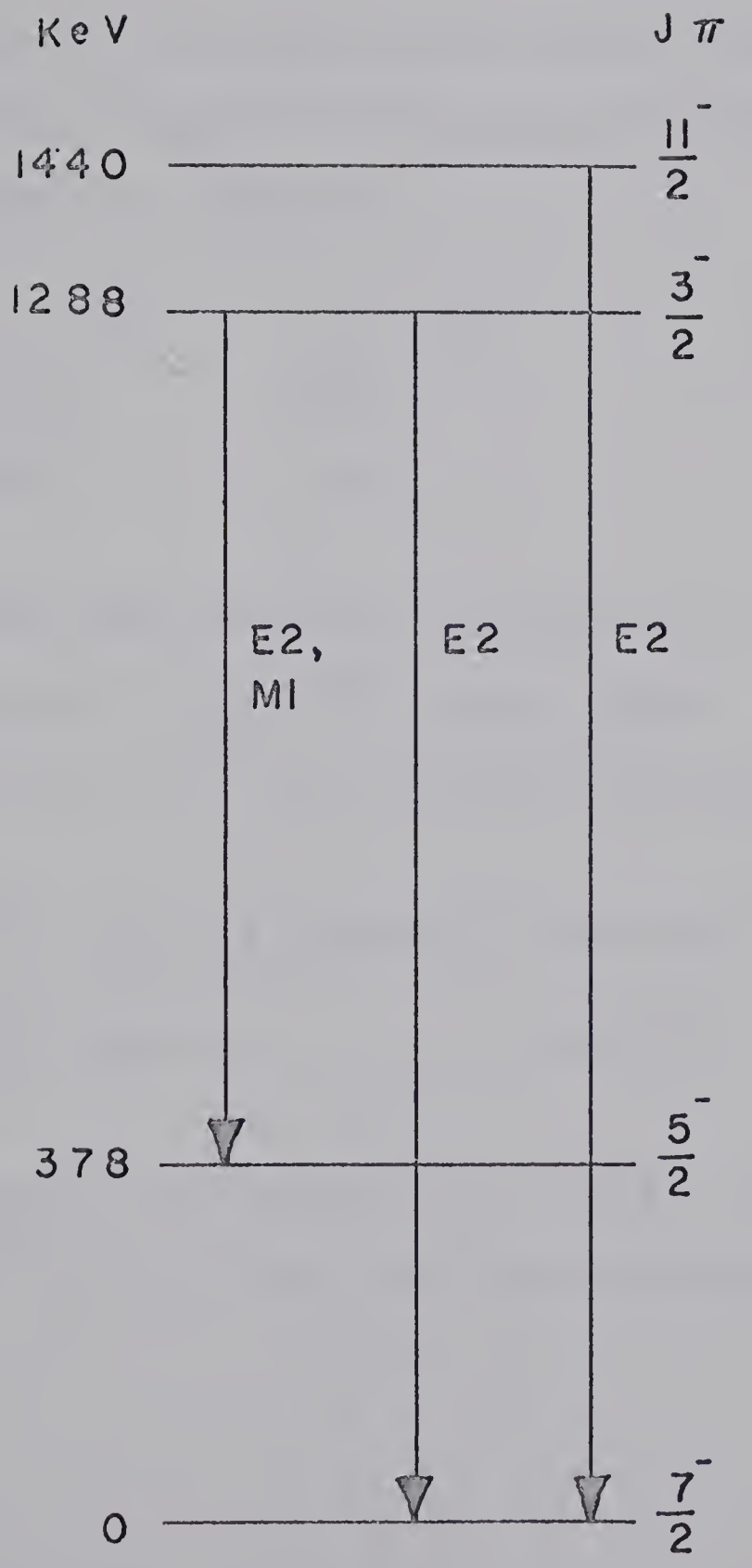

FIGURE 12

1440 KeV (1440 $\longrightarrow$ 0)

1288 (1288 $\longrightarrow$ 0)

910 (1288 $\longrightarrow$ 378)

and figure 12 shows the level scheme considered.

Full kinematic shifts were determined for the three gamma ray energies:

910 KeV 3.003 KeV

1288 4.250

1440 4.694

The gain shift was determined by calculating the centroids of the ^{60}Co source peaks. The centroids obtained for the ^{60}Co 1.333 MeV line were:

0° centroid (channel) = 880.274 ± 0.08

90° centroid = 878.736 ± 0.006 ;

The difference was found to be 1.538 ± .086 channels. For the ^{60}Co 1.172 MeV line the centroids were:

0° centroid (channel) = 774.943 ± .08

90° centroid = 773.410 ± .006.

Here the difference was 1.533 ± .086 channels. Thus the 0° spectrum was shifted upwards by 1.535 ± .17 channels. Also the energy calibration for both spectra using the source lines was obtained by observing that

105.33 channels = 160 KeV

or 1 channel = 1.517 KeV.

The same centroid analysis was applied to the three gamma ray peaks.

The 1288 $\longrightarrow$ 0 transition (figure 13)

0° centroid = 602.090 ± 0.21

90° = 600.468 ± 0.09

Figure 13 and Figure 14. The background subtracted peaks from the 0° and 90° runs for the three transitions are shown. The background for the 0° peaks amounts to an almost constant 10 counts per channel. For the 1288 $\longrightarrow$ 0 and 1440 $\longrightarrow$ 0 90° peaks, the background is about 3000 counts per channel and for the 1288 $\longrightarrow$ 378 90° peak it is 6900 counts per channel. The uncorrected shifts are also indicated.

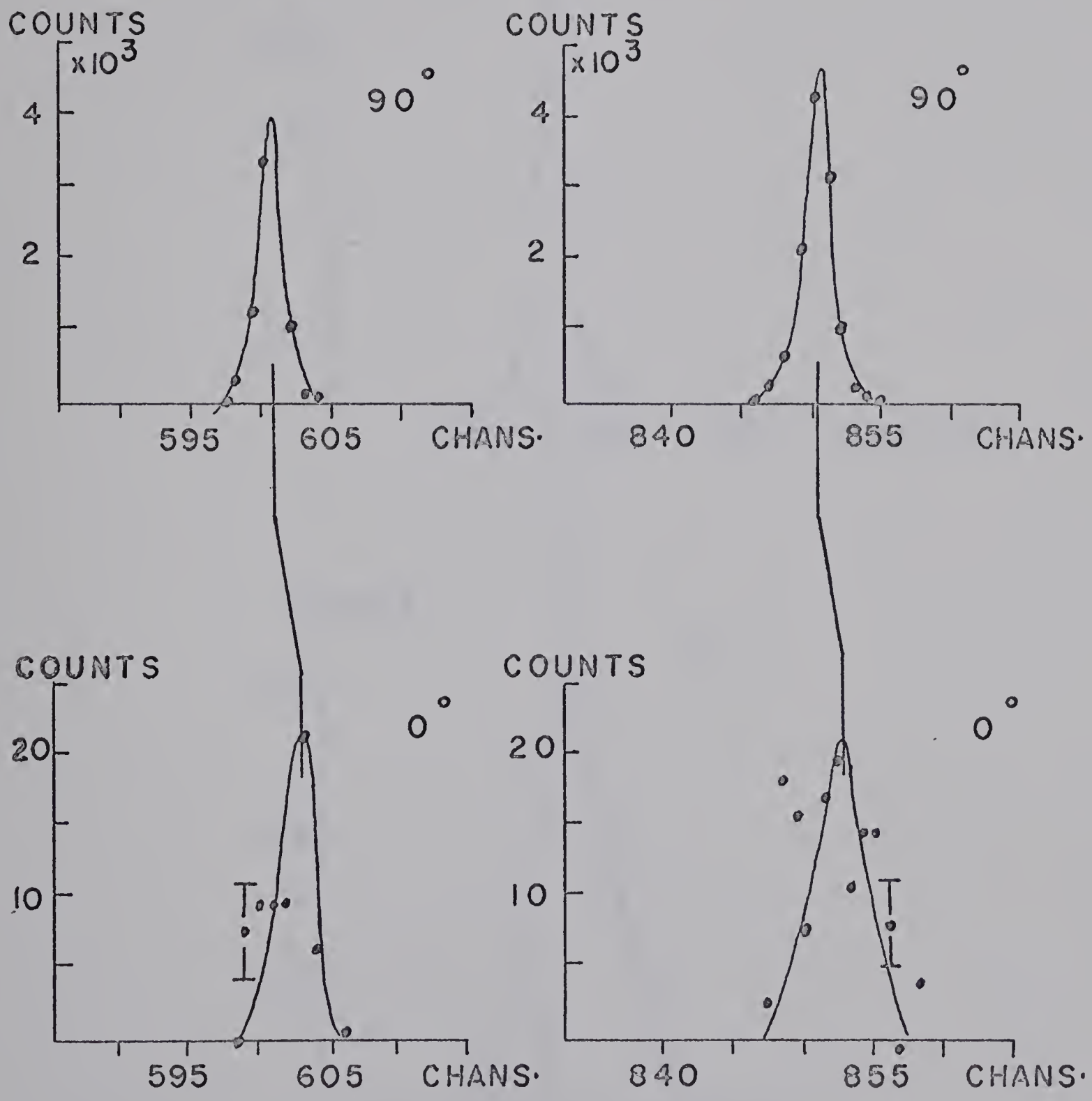
1288 → 378
1288 → 0
COUNTS
x10^3
90°
4
2
595
605
CHANS.
840
855
COUNTS
0°
20
10

FIGURE 13

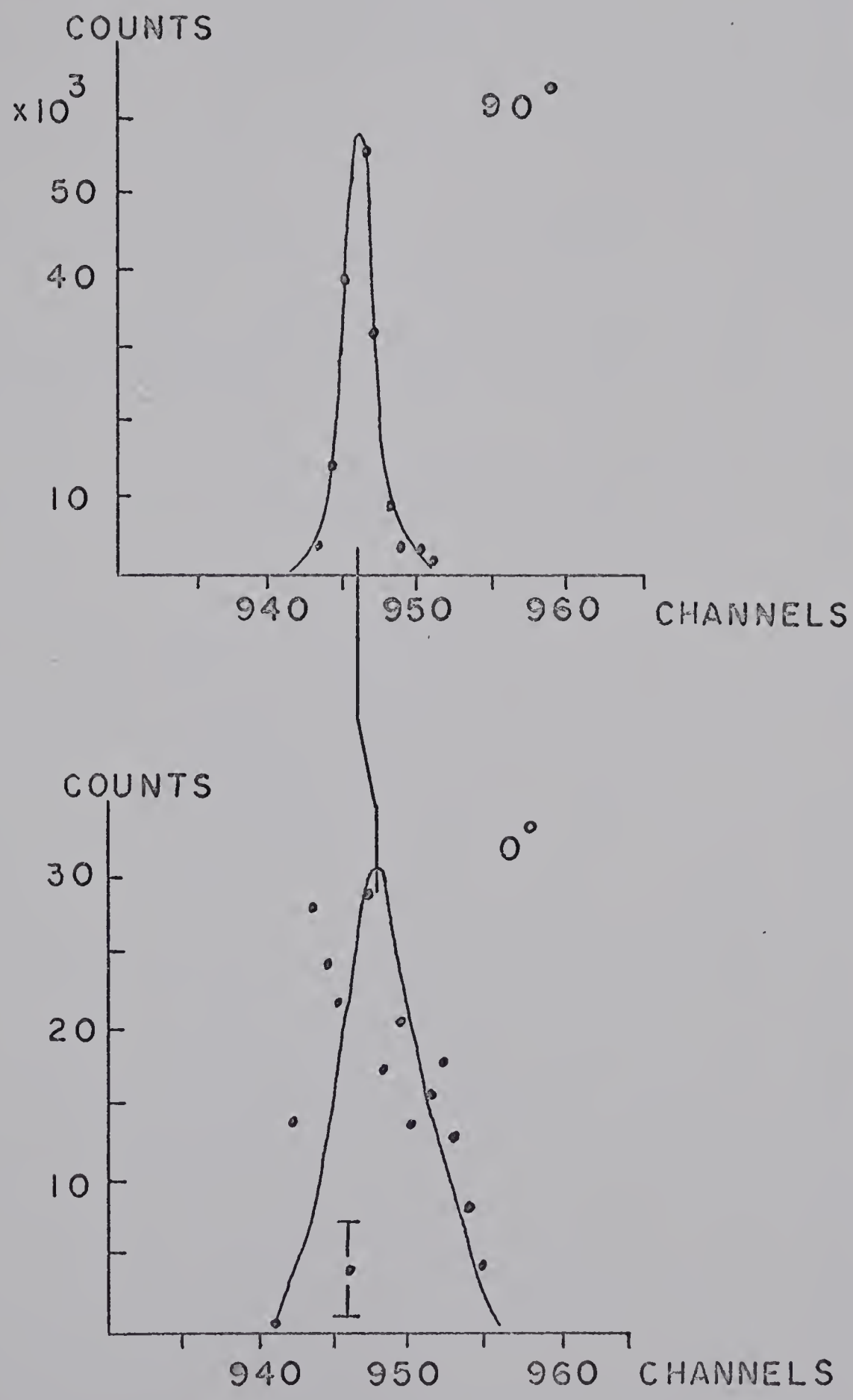
1440 → 0
COUNTS
x10^3
50
40
10
90°
940
950
960
CHANNELS
COUNTS
30
20
10
0°
940
950
960
CHANNELS

FIGURE 14

Figure 15. The $F(\tau)$ function is plotted against the lifetime τ (in p.s.) for the case of ^{53}Mn recoil nuclei slowing down in the Cr backing. The following experimental points with $F(\tau)$ errors are are shown:

(1) 1288 $\longrightarrow$ 378 and 1288 $\longrightarrow$ 0 transitions;

(2) 1440 $\longrightarrow$ 0 transition.

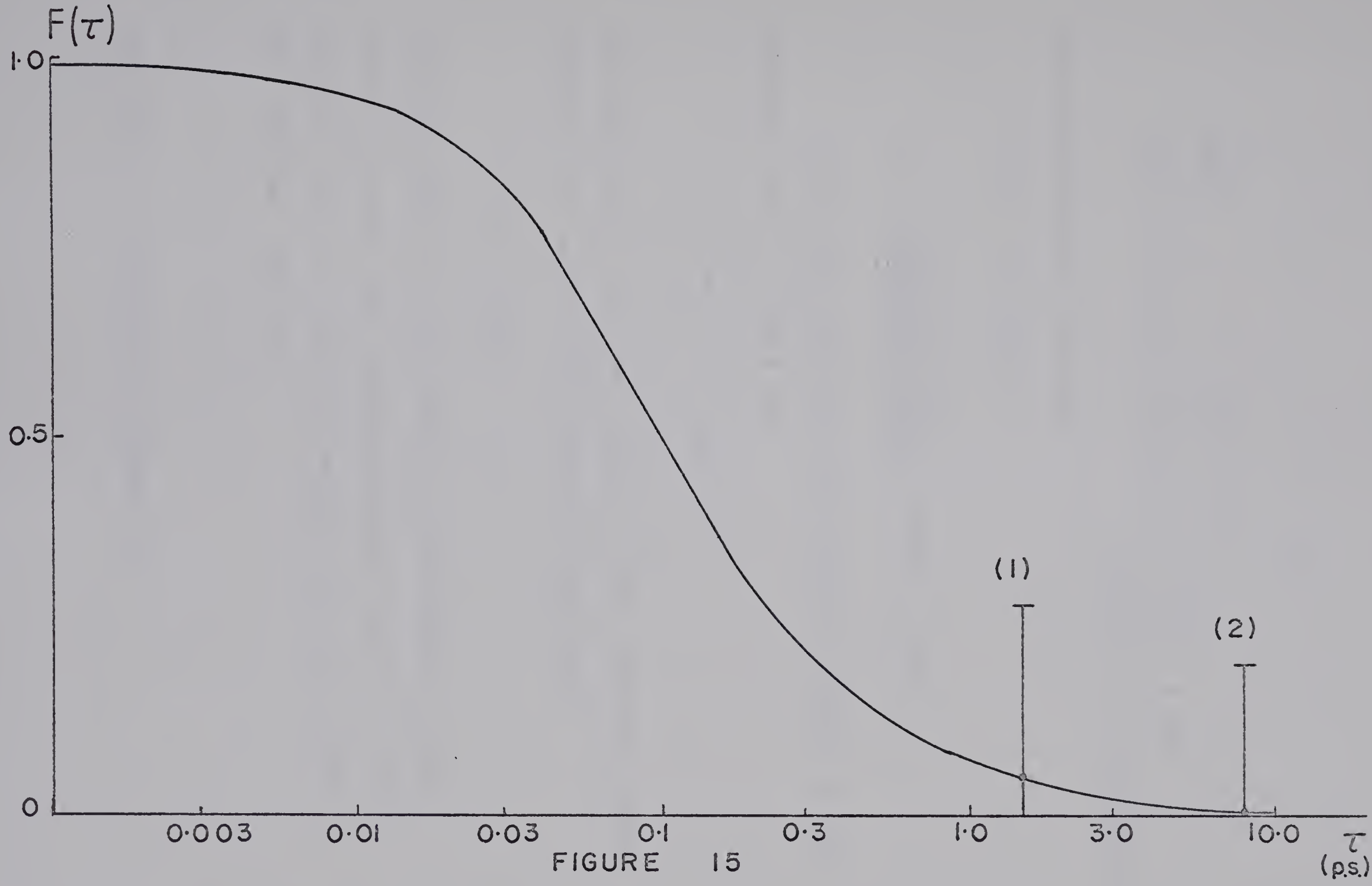

FIGURE 15

shift = 1.622 ± 0.30

shift with gain correction = 1.622 - 1.535

= 0.087 ± 0.47 channels.

The observed shift was then

0.132 ± .71 KeV .

$$F(\tau) = \frac{\text{observed shift}}{\text{kinematic shift}} = 0.044 \pm 0.236 .$$

Having used the $F(\tau)$ curve given in figure 15 the lifetime for this level is

$$\tau \approx 1.5 \; {}^{+\infty}_{-1.3} \quad \text{p.s.}$$

The large upper and lower bounds on the lifetime result from the $F(\tau)$ error since for this transition

$$0 < F(\tau) < 0.28.$$

In cases where the data falls in the region of every small $F(\tau)$ such that the experimental error is larger than $F(\tau)$ one, in practice, accepts the lower bound on the lifetime. That is,

$$\tau > 0.2 \quad \text{p.s.}$$

The 1288 $\longrightarrow$ 0 transition (figure 13)

0° centroid = 851.795 ± 0.30

90° = 850.144 ± 0.12

difference = 1.651 ± 0.42 channels

corrected shift = 0.116 ± 0.590 channels

= 0.176 ± 0.894 KeV

$F(\tau) = 0.042 \pm 0.211.$

Thus,

$$\tau = 1.5 \; {}^{+\infty}_{-1.3}$$

or

$$\tau > 0.2 \text{ p.s.}$$

The 1440 $\longrightarrow$ 0 transition (figure 14)

0° centroid = 947.574 ± 0.39

90° = 946.019 ± 0.06

difference = 1.555 ± 0.43 channels

corrected shift = 0.020 ± 0.62 channels

= 0.030 ± 0.940 KeV

$F(\tau) = 0.006 \pm 0.190.$

Thus,

$$\tau = 8 \; {}^{+\infty}_{-7.7}$$

or

$$\tau > 0.3 \text{ p.s.}$$

Transition	τ exptl.(p.s.)	Weisskopf(p.s.)
1288 ⟶ 378 $3/2^- \longrightarrow 5/2^-$	$1.5^{+\infty}_{-1.3}$	110 (E2) 0.042 (M1)
1288 ⟶ 0 $3/2^- \longrightarrow 7/2^-$	$1.5^{+\infty}_{-1.3}$	19 (E2)
1440 ⟶ 0 $11/2^- \longrightarrow 7/2^-$	$8.0^{+\infty}_{-7.7}$	11 (E2)

Table 1

These results along with the single particle or Weisskopf estimates of the lifetimes are summarized in table 1. For the 1288 ⟶ 378 transition it seems as though E2 radiation is enhanced and M1 radiation is retarded. The other two transitions are pure E2. Furthermore, since the Weisskopf estimate for E1 radiation is so low (retarded by a factor of 10^{-4} from E2) compared to the experimental limit for the 1288 ⟶ 378 transition and since the other transitions are pure E2, the parity for the first three excited levels are verified.

5.3 Throughout the experiment the problem of low coincidence rates was apparent and resulted in the poor statistics of the 0^{o} spectrum. This condition may be improved first by taking care to see that the neutron detector discriminator level is set just above the self-triggering point since its inherent neutron threshold is approximately 800 KeV, and a level much above this ($\approx$ 1.5 MeV) will result in a loss of high energy coincidence gamma rays. Also, the bias should be applied several hours before run time to avoid immediate drifting of the discriminator level. The excessive gamma ray count rate in the neutron detector indicates that the $\frac{1}{8}$" lead shielding is not thick enough to reduce the flux of low energy gamma rays and should be increased (perhaps to ½").

Secondly, difficulty was encountered in trying to get all the signals going to the coincidence units to arrive at the same time since adjustment of an SCA window disturbed the timing. This problem can be minimized by strobing the SCA's instead of the TAC's as shown in figure 7. Also, the neutron window on the n-γ time spectrum should be set as close to the gamma ray peak as possible to include the high energy neutrons that populate the lower levels of the residual neucleus.

Finally, modifications should be made to the target pot assembly including better beam collimators and the

electrical isolation of the target from the target pot so that the current indicator actually registers a beam on the target instead of on the entire assembly. The only indicator of a beam on a target during the experiment was the gamma ray ratemeter.

In conclusion, the adoption of these improvements will serve to increase the n-γ coincidence rate (as has been shown in a later experiment where the ratio of gamma ray to neutron counts in the neutron detector has been decreased from 15 to 1 to 3 to 1), thus making the present system employing coincidence methods very useful in measuring Doppler shifts for DSAM lifetime studies.

BIBLIOGRAPHY

Af 65 V.V. Afrosimov, et al., Soviet Physics - Tech. Phys. 9 (1965) 1248, 1256, and 1265.

Bo 48 N. Bohr, Mat. Fys. Medd. Dan. Vid. Selsk. 18 No. 8 (1948).

Bl 66 A.E. Blaugrund, Nuclear Physics 88 (1966) 501.

Br 59 F.D. Brooks, Nucl. Instr. and Meth. 4 (1959) 151.

Da 65 P. Dahl and J. Magyer, Phys. Rev. 140 (1965) A1420.

De 63 G. Dearnaley and D.C. Northrop, "Semiconductor Counters for Nuclear Radiations", E. and F.N. Spon Limited, London, 1963.

Ev 65 E. Everhart and Q.C. Kessel, Phys. Rev. Letters 14 (1965) 484.

Fi 58 O.B. Firsov, JETP, 6 (1958) 534.

Fi 58 O.B. Firsov, JETP, 7 (1958) 308.

Fi 59 O.B. Firsov, JETP, 9 (1959) 1076.

Ke 65 Q.C. Kessel, et al., Phys. Rev. Letters 14 (1965) 484.

Le 50 H.W. Lewis, Phys. Rev. 78 (1950) 526.

Li 61 J. Lindhard and M. Scharff, Phys. Rev. 124 (1961) 128.

Li 63 J. Lindhard, M. Scharff, and H.E. Schiott, Mat. Fys. Medd. Dan. Vid. Selsk. 33, No. 14 (1963).

Mo 62 G.H. Morgan and E. Everhart, Phys. Rev. 128 (1962) 667.

Mo 64 P.M. Morse, "Thermal Physics", rev. ed., W.A. Benjamin, New York, 1964.

No 60 L.C. Northcliffe, Phys. Rev. 120 (1960) 1744.

No 63 L.C. Northcliffe, Ann. Rev. Nucl. Sci. 13 (1963) 67.

Pi 64 G.R. Piercy, et al., Can. J. Phys. 42 (1964) 1116.

Po 61 D.I. Porat and K. Ramavataram, Proc. Phys. Soc. 78 (1961) 1135.

Ra 64 C. Ratz and S. Smock, Phys. Rev. 137 (1964) A347.

Re 55 H.L. Reynolds et al., Phys. Rev. 98 (1955) 474.

Re 61 G.T. Reynolds and F. Reines, "Methods of Experimental Physics", V.5, Academic Press, N.Y., 1961.

Ro 65 P. Rol, et al., Proc. 7th International Conference on PHenomena in Ionized Gases. Belgrade (1965).

Ro 69 B.C. Robertson, Ph.D. Thesis, Oxford University (1969).

Sa 68 E. Sakai and T.A. McMath, Nucl. Instr. and Meth. 64 (1968) 132.

Sy 64 K.R. Symon, "Mechanics", Addison-Wesley Publishing Company, Inc., Palo Alto, 1953.

Ta 51 C.J. Taylor et al., Phys. Rev. 84 (1951) 1034.

Appendix 1

The Angular Distribution Function $F(\phi,s)$

Suppose a charged particle is moving in a medium containing N atoms per unit volume. Its position is given by x and its direction of motion is given by the unit vector $\hat{\phi}$. The scattering cross-section per unit solid angle for the particle in the material is $\sigma(|\hat{\phi}-\hat{\phi}'|)$ (that is, the cross-section for the particle changing its direction from $\hat{\phi}$ to $\hat{\phi}'$, the angle between these two unit vectors being the scattering angle θ). The distribution function of the particle will be denoted by $f(\vec{x},\hat{\phi},s)$, where s is the arc length traversed by the moving particle.

Assume now, that at some position $\vec{x}$, arc length s, and direction $\hat{\phi}$, the particle suffers a collision which changes its direction to $\hat{\phi}'$. The distribution function changes from $f(\vec{x},\hat{\phi},s)$ to $f(\vec{x},\hat{\phi}',s)$. Conservation of particles demands that the change in f due to the change in direction of the particle plus the sum of the changes in f as functions of $\vec{x}$ and s, must be equal to zero. Or, symbolically:

$$\nabla_{\vec{x},s,\hat{\phi}} \cdot f = 0 \quad . \tag{1}$$

The divergence of f with respect to the first two variables will clearly be

$$\frac{\partial f}{\partial s} + \hat{\phi} \cdot \nabla f \quad . \tag{2}$$

The change of f with $\hat{\phi}$ will be given by the integral of $f(\vec{x},\hat{\phi}',s) - f(\vec{x},\hat{\phi},s)$ weighted by the cross-section for scattering from $\hat{\phi}$ to $\hat{\phi}'$ over all final directions $\hat{\phi}'$: Thus

$$\frac{\partial f}{\partial s} + \hat{\phi}. \nabla f = N \int [f(\vec{x},\hat{\phi}',s)-f(\vec{x},\hat{\phi},s)]\ \sigma(|\hat{\phi}-\hat{\phi}'|)\ d\hat{\phi}' \tag{3}$$

which is of course the diffusion equation (1) with the last term transposed. The boundary condition of this equation will be that f be unity at the origin:

$$f(\vec{x},\hat{\phi},0) = \delta(\vec{x})\ \delta(\hat{\phi}) \quad . \tag{4}$$

$\hat{\phi} = 0$ means that the particle at the origin is assumed to be moving in the incident beam direction (z-axis). f is now expanded in terms of the spherical harmonics in $\hat{\phi}$:

$$f(\vec{x},\hat{\phi},s) = \sum_{\substack{\ell m \\ =0}}^{\infty} f_{\ell m}(\vec{x},s)\ Y_{\ell m}(\hat{\phi}) \quad . \tag{5}$$

Hence, one has from (3)

$$\sum_{\ell m} \frac{\partial f_{\ell m}}{\partial s} Y_{\ell m}(\hat{\phi}) + \sum_{\ell m} (\hat{\phi}\, Y_{\ell m}(\hat{\phi})) \cdot \nabla f_{\ell m}$$

$$= N \sum_{\ell m} f_{\ell m} \int [Y_{\ell m}(\hat{\phi}') - Y_{\ell m}(\hat{\phi})]\sigma(|\hat{\phi}-\hat{\phi}'|)d\hat{\phi}' . \quad (6)$$

Multiplying (6) from the left by $Y^*_{ij}(\hat{\phi})$ and then integrating with respect to $\hat{\phi}$ gives,

$$\frac{\partial f_{ij}}{\partial s} + \sum_{\ell m} \nabla f_{\ell m} \cdot \int Y^*_{ij}(\hat{\phi})\, \hat{\phi}\, Y_{\ell m}(\hat{\phi})\, d\hat{\phi}$$

$$= N \sum_{\ell m} f_{\ell m} \int\int Y^*_{ij}(\hat{\phi})[Y_{\ell m}(\hat{\phi}') - Y_{\ell m}(\hat{\phi})]\sigma(|\hat{\phi}-\hat{\phi}'|)d\hat{\phi}\, d\hat{\phi}'$$

$$= N \sum_{\ell m} f_{\ell j} \int [P_\ell(\cos\theta) - 1]\, \delta_{\ell i}\, \sigma(\theta)\, d\hat{\phi} \quad (7)$$

using the addition theorem for spherical harmonics and the orthonormality condition.

Define:

$$Q^{\ell m}_{ij} \equiv \int Y^*_{ij}(\hat{\phi})\, \hat{\phi}\, Y_{\ell m}(\hat{\phi})\, d\hat{\phi} \quad .$$

The right side of (7) becomes

$$N f_{ij} \int_0^{2\pi} \int_0^{\pi} [P_i(\cos\theta) - 1]\, \sigma(\theta)\, \sin\theta\, d\theta\, d\theta$$

$$= 2\pi N f_{ij} \int_0^{\pi} [P_i(\cos\theta) - 1]\, \sigma(\theta)\, \sin\theta\, d\theta$$

$$\equiv - f_{ij}\, K_i \quad (8)$$

where K_i is equal to $-2\pi N$ times the integral. Thus (7) becomes

$$\frac{\partial f_{ij}}{\partial s} + K_i f_{ij} = - \sum_{\ell m} \nabla f_{\ell m} \cdot Q_{ij}^{\ell m} \qquad (9)$$

the boundary condition of which is given by

$$f_{io}(\vec{x},0) \equiv f_i(\vec{x},0) = \delta(\vec{x})\ Y_{io}(0)$$

$$= \left(\frac{2i+1}{4\pi}\right)^{\frac{1}{2}} \delta(\vec{x}) \ . \qquad (10)$$

j (also m) has been set equal to zero since the cylindrical symmetry of the problem demands this. (Note that because m=j=0, ℓ=i). Thus, one has

$$Q_{\ell o}^{\ell o} = \int_{-1}^{1} \hat{\phi}\ P_\ell(\hat{\phi})\ d(\hat{\phi}) = 0 \qquad (11)$$

since the integrand is an odd function. Putting these results into (9) one has

$$\frac{\partial f_\ell(\vec{x},s)}{\partial s} + K_\ell\ f_\ell(\vec{x},s) = 0 \ . \qquad (12)$$

Define

$$\int f_\ell(\vec{x},s)\ d\vec{x} = F_\ell(s) \ .$$

Integrating (12) over all space will then give

$$\frac{\partial F_\ell(s)}{\partial s} + K_\ell\ F_\ell(s) = 0 \qquad (13)$$

the solution of which is given by

$$F_\ell(s) = \left(\frac{2\ell+1}{4\pi}\right)^{\frac{1}{2}} \exp\left(-\int_0^s K_\ell \, ds\right) \tag{14}$$

where $F_\ell(s)$ satisfies the boundary condition (10) through the relation

$$F_\ell(0) = \int f_\ell(\vec{x},0)\, d\vec{x} = \left(\frac{2\ell+1}{4\pi}\right)^{\frac{1}{2}} \delta(\vec{x})\, d\vec{x}$$

$$= \left(\frac{2\ell+1}{4\pi}\right)^{\frac{1}{2}} .$$

Returning to (5) one finds that

$$F_\ell(\hat{\phi},s) \equiv \int f_\ell(\vec{x},\hat{\phi},s)\, d\vec{x}$$

$$= \sum_{\ell,m=0} \int f_\ell(\vec{x},s)\, d\vec{x}\, \left(\frac{2\ell+1}{4\pi}\right)^{\frac{1}{2}} P_\ell(\cos\theta)$$

$$= \frac{1}{4\pi} \sum_{\ell=0}^{\infty} (2\ell+1)\, P_\ell(\cos\theta) \exp\left(-\int_0^s K_\ell \, ds\right) . \tag{15}$$

Appendix 2

Derivation of cos ϕ

Recall,

$$\cos \phi = \frac{r + a}{(1 + 2ra + r^2)^{\frac{1}{2}}} \qquad (1)$$

where $a = \cos \Theta$.

The generating function for Legendre polynomials is given by

$$(1 - 2ra + r^2)^{-\frac{1}{2}} = \sum_{n=0}^{\infty} P_n(a)\, r^n \quad . \qquad (2)$$

From the properties of the Legendre polynomials one has that

$$P_n(-a) = (-1)^n P_n(a) \qquad (3)$$

and the recursion relation

$$(2n + 1)\, a\, P_n(a) = (n + 1)\, P_{n+1}(a) + n\, P_{n-1}(a). \qquad (4)$$

Thus,

$$(1 + 2ra + r^2)^{-\frac{1}{2}} = \sum_{n=0} (-1)^n P_n(a)\, r^n \qquad (5)$$

and

$$\cos\phi = (r + a) \sum_{n=0} (-1)^n P_n(a)\, r^n$$

$$= \sum_{n=0} (-1)^n P_n(a)\, r^{n+1} + \sum_{n=0} (-1)^n a\, P_n(a)\, r^n$$

$$= -\sum_{n=1} (-1)^n P_{n-1}(a)\, r^n + a + \sum_{n=1} (-1)^n a\, P_n(a)\, r^n. \qquad (6)$$

Since n is a dummy index it has been replaced by n-1 in the first term causing the summation to start from n=1. But

$$\sum_{n=1} (-1)^n a\, P_n(a)\, r^n = \sum_{n=1} (-1)^n \left[\frac{n+1}{2n+1} P_{n+1}(a) + \frac{n}{2n+1} P_{n-1}(a)\right] r^n \qquad (7)$$

so that

$$\cos\phi = a + \sum_{n=1} (-1)^n \left\{\frac{n+1}{2n+1} P_{n+1}(a) + \left[\frac{n}{2n+1} - 1\right] P_{n-1}(a)\right\} r^n \qquad (8)$$

using (6) and (7). Or,

$$\cos\phi = P_1(\cos\theta) + \sum_{n=1} (-1)^n \frac{n+1}{2n+1} \times$$

$$\times \left[P_{n+1}(\cos\theta) - P_{n-1}(\cos\theta)\right] r^n . \qquad (9)$$

$$r < 1$$

For $r > 1$ the generating function is given by

$$(1 - 2ra + r^2)^{-\frac{1}{2}} = \sum_{n=0}^{\infty} P_n(a) \left(\frac{1}{r}\right)^{n+1}$$

and the rest of the derivation proceeds in an entirely analogous manner and gives

$$\cos \phi = 1 + \sum_{n=1}^{\infty} (-1)^n \frac{n}{2n+1} [P_{n+1}(\cos \theta) - P_{n-1}(\cos \theta)] \times$$

$$\times \left(\frac{1}{r}\right)^{n+1} . \quad r > 1 \qquad (10)$$